Geometrical optics analysis of the structural imperfection of retroreflection corner cubes with a nonlinear conjugate gradient method

Hwi Kim,[1] Sung-Wook Min,[2,*] and Byoungho Lee[1]

[1]School of Electrical Engineering, Seoul National University, Gwanak-Gu Shinlim-Dong, Seoul 151-744, Korea

[2]Department of Information Display, College of Science, Kyung Hee University, Hoeki-dong, Dongdaemoon-ku Seoul 130-701, Korea

*Corresponding author: mins@khu.ac.kr

Received 2 July 2008; revised 27 September 2008; accepted 30 September 2008; posted 3 October 2008 (Doc. ID 98133); published 27 November 2008

Geometrical optics analysis of the structural imperfection of retroreflection corner cubes is described. In the analysis, a geometrical optics model of six-beam reflection patterns generated by an imperfect retroreflection corner cube is developed, and its structural error extraction is formulated as a nonlinear optimization problem. The nonlinear conjugate gradient method is employed for solving the nonlinear optimization problem, and its detailed implementation is described. The proposed method of analysis is a mathematical basis for the nondestructive optical inspection of imperfectly fabricated retroreflection corner cubes. © 2008 Optical Society of America

OCIS codes: 080.0080, 080.2720, 230.5480.

1. Introduction

Retroreflection is the well-known reflection phenomenon [1] that the optical rays radiated from an optical source are reflected back to the optical source along the inverse directions of the incident rays. For realizing retroreflection, specifically designed optical devices, retroreflectors, are used. Several types of retroreflectors and their optical properties have been investigated [1–7]. The most popular type of retroreflector is the corner cube, schematically depicted in Fig. 1(a). The conventional corner cube is composed of four facets, including one incidence triangular facet, $\triangle P_1P_2P_3$, and three total internal reflection facets, $\triangle P_1P_2P_5$, $\triangle P_2P_3P_5$, and $\triangle P_3P_1P_5$. Point P_4 is the foot of the perpendicular of P_5 on the incidence facet. If the dihedral angles between three reflection facets are exactly 90°, the incident ray is reflected consecutively at three reflection facets and returns to the light source along the incidence direction as shown in Fig. 1(a). Retroreflection by a corner-cube structure is used in many practical applications requiring accurate retroreflection, such as positioning and guidance systems [8–10], wavefront correction [11], optical communications [12], and traffic control signs [13–15]. In particular, the retroreflectors are considered a key element of a new application, head-mounted projective display, wherein great technology advancements have been made in recent years [16–22].

Although the structural condition of the perfect retroreflection corner cube is known [23], imperfect fabrication of corner cubes is inevitable in practice. In this paper, the structural imperfection means that the apex point of the fabricated corner cube, P_5', deviates from the apex point P_5 of the perfect corner cube. It is well known that when a corner-cube structure has a structural error, the imperfect retroreflection corner cube will generate six-beam reflection patterns as illustrated in Fig. 1(b). As the structural error becomes bigger, the distances among the six reflection beams increase. Direct measurement of the structural imperfection is not easy and often requires

0003-6935/08/346453-17$15.00/0

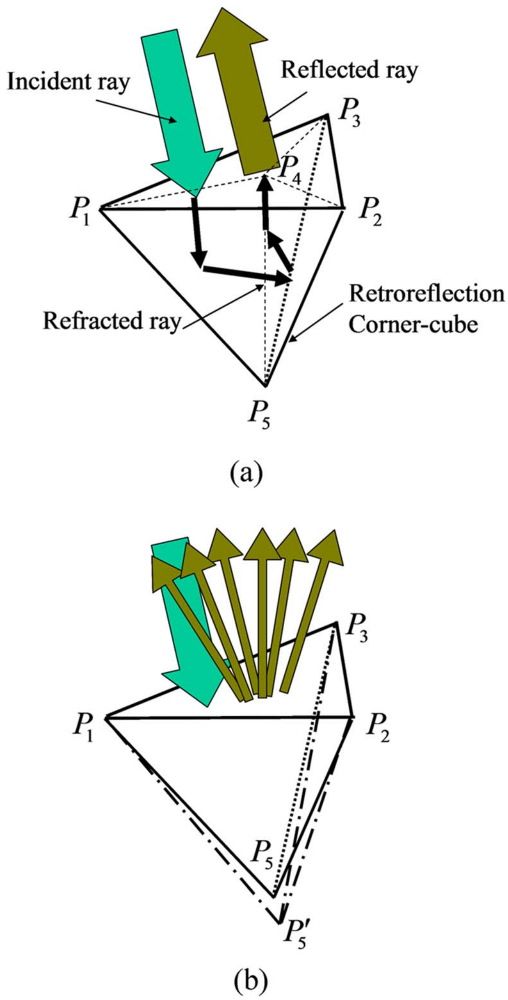

Fig. 1. (Color online) (a) Retroreflection by a perfect corner cube and (b) retroreflection by an imperfect corner cube.

destruction, since corner cubes are fabricated on a microscale and are formed as a sheet composed of a periodic array of identical corner cubes. However, the observable six-beam reflection pattern generated from the imperfect corner cube is optically measurable data that can be used for nondestructively analyzing the structural imperfection of the corner cube. Theoretically, two-beam and four-beam reflection patterns can occur with imperfect corner cubes as special cases of the six-beam reflection pattern. The detailed analysis of this reflection pattern classification is addressed in the main part of this paper.

Regarding the analysis of imperfect corner cubes, we can pose a forward analysis problem and an inverse analysis problem separately. The forward analysis problem concerns the optical reflection characteristics of a corner cube whose structure is known *a priori*. Optical properties such as effective retroreflection area [23], reflection direction, and so on, are interesting aspects with respect to the forward analysis problem. The inverse analysis problem concerns the structural analysis of the corner cube itself, whose structure is not known *a priori*. There little literature on the inverse analysis of retroreflection corner cubes. In this paper, we deal with the inverse analysis problem, where from measurable data, such as optical reflection patterns and power, we analyze the structure of the examined corner cube, such as the position of the apex point P_5'.

In this paper, we describe a mathematical method to inversely extract the position of the apex point, P_5', of the examined imperfect retroreflection corner cubes by using the reflection pattern data. In the analysis, the mathematical relationship between the six-beam reflection pattern and the position of the apex point of the imperfect corner cube is formulated as six nonlinear algebraic equations. We set the structural error $(\hat{x}, \hat{y}, \hat{z})$ of the apex point as the unknown variables, and then the unknown variables $(\hat{x}, \hat{y}, \hat{z})$ appear in the nonlinear algebraic equations. As a result, the inverse structural analysis of the imperfect retroreflection corner cubes is equivalent to obtaining the solution $(\hat{x}, \hat{y}, \hat{z})$ from the nonlinear algebraic equation. In general, nonlinear algebraic equations have several solutions, and there is no general method to solve the equations. Thus, numerical optimization techniques are often employed to solve the nonlinear algebraic equations. In this paper, the nonlinear conjugate gradient method (NCGM) is employed for solving the inverse structural analysis problem, and its detailed implementation is described. Fortunately, it is advantageous that the inverse analysis problem of an imperfect corner cube has a single solution, and the convergence of the NCGM is confirmed.

This paper is organized as follows. In Section 2, the geometrical optics model of single corner cube is developed. The mathematical relationship between the corner-cube structural error and the reflection pattern is derived with the geometrical optics model. In Section 3, the NCGM for the structural analysis of single corner cube is formulated, and numerical results are presented. In Section 4, concluding remarks are provided.

2. Geometrical Optics Model of a Single Corner Cube

In this section, the geometrical optics model of single corner cube is developed. Let a single corner cube with a triangle incidence facet be in the Cartesian coordinate system shown in Fig. 2. The corner cube is composed of an incidence facet and three reflection facets drawn by the pairs of three vertices, (P_1, P_2, P_3), (P_5, P_1, P_2), (P_5, P_2, P_3), and (P_5, P_3, P_1), which are denoted T_0, T_1, T_2, and T_3, respectively. It is assumed that we can only observe the top view of the corner cube using a microscope. Thus, by measuring the lengths of observable edges, l_{12}, l_{13}, and l_{23}, of the fabricated corner cube, we can obtain the coordinates of the vertices of the examined corner cubes, $P_1(x_1, y_1, 0)$, $P_2(x_2, y_2, 0)$, and $P_3(x_3, y_3, 0)$, which are given, respectively, by

$$P_1: \ (x_1, y_1) = (0, 0), \tag{1a}$$

$$P_2: \ (x_2, y_2) = (l_{12}, 0), \tag{1b}$$

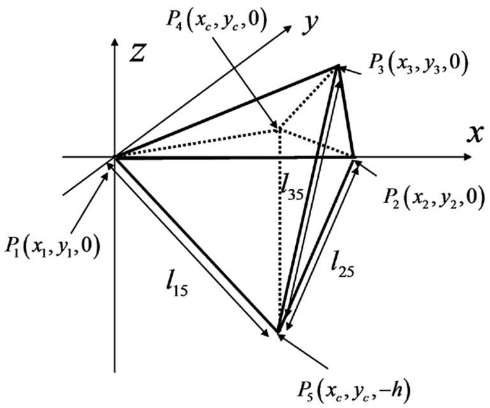

(a)

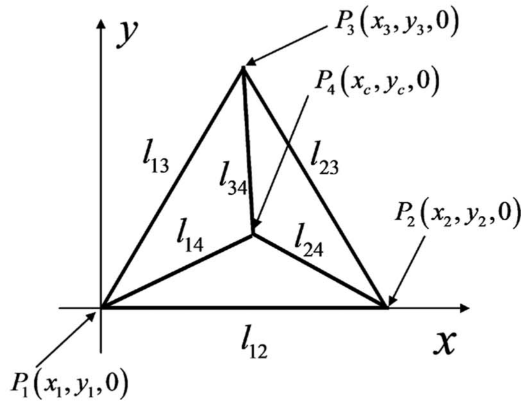

(b)

Fig. 2. Corner cube in the Cartesian coordinate system: (a) side-view, (b) top-view.

$$P_3:\ (x_3, y_3) = \left(\frac{l_{12}^2 + l_{13}^2 - l_{23}^2}{2l_{12}}, \sqrt{l_{13}^2 - x_3^2}\right)$$
$$= \left(\frac{l_{12}^2 + l_{13}^2 - l_{23}^2}{2l_{12}}, \frac{\sqrt{(l_{12}+l_{23}+l_{13})(l_{12}-l_{23}+l_{13})(l_{12}+l_{23}-l_{13})(-l_{12}+l_{23}+l_{13})}}{2l_{12}}\right). \tag{1c}$$

With only the top view of the corner cube, we cannot directly obtain the edges, l_{14}, l_{24}, and l_{34}. These edge lengths are nonmeasurable data. Let the point $(\bar{x}_c, \bar{y}_c, -\bar{h})$ be the coordinate of the apex point of the perfect corner cube structure for a normal incidence light wave (see Appendix A and [23]).

Let the structural error of the apex point of imperfect corner cube be denoted $(\hat{x}, \hat{y}, \hat{z})$. Then the apex point P_5 of the imperfect structure is given by $P_5(x_c, y_c, -h) = (\bar{x}_c + \hat{x}, \bar{y}_c + \hat{y}, -(\bar{h} + \hat{z}))$. According to the equation of a plane with the normal vector (a, b, c), $ax + by + cz + d = 0$, the normal vectors of T_1, T_2, and T_3, (a_1, b_1, c_1), (a_2, b_2, c_2), and (a_3, b_3, c_3) are given, respectively, as

$$(a_1, b_1, c_1) = (0, -x_2 h, -x_2 y_c) \quad \text{for } T_1, \tag{2a}$$

$$(a_2, b_2, c_2) = (y_3 h, (-x_3 + x_2)h, -x_2 y_3 + y_3 x_c + (x_2 - x_3) y_c) \quad \text{for } T_2, \tag{2b}$$

$$(a_3, b_3, c_3) = (-y_3 h, x_3 h, y_c x_3 - y_3 x_c) \quad \text{for } T_3. \tag{2c}$$

Let us define the reflection transform $\mathbf{\Gamma}_i$ $(i = 1, 2, 3)$ representing the mathematical transform of an incident ray vector, (k_x, k_y, k_z), to the reflection ray vector, $(k_{r,x}, k_{r,y}, k_{r,z})$ by the reflection facet T_i, with the form (see Appendix B)

$$(k_{r,x}, k_{r,y}, k_{r,z})^t = \mathbf{\Gamma}_i (k_x, k_y, k_z)^t. \tag{3}$$

In addition, let us consider the process of refraction through the incidence facet T_0. If an optical ray with the incidence angle of θ and the azimuth angle of ϕ is incident on the incidence facet of a corner cube, the direction vector $(k_{i,x}, k_{i,y}, k_{i,z})$ of the incident optical ray is represented by

$$(k_{i,x}, k_{i,y}, k_{i,z}) = (\cos\phi \sin\theta, \sin\phi \sin\theta, -\cos\theta). \tag{4a}$$

The refracted ray vector (k_x, k_y, k_z) in a material with a refractive index of n, is given, from Snell's law, as

$$(k_x, k_y, k_z) = \frac{1}{n}\left(\cos\phi \sin\theta, \sin\phi \sin\theta, -\sqrt{n^2 - (\sin\theta)^2}\right)$$
$$= (\cos\phi' \sin\theta', \sin\phi' \sin\theta', -\cos\theta'), \tag{4b}$$

where θ' and ϕ' are the refraction incidence angle and the refraction azimuth angle, respectively. From Eqs. (4a) and (4b), we can define the nonlinear refraction transformation $\mathbf{\Gamma}_0$ from $(k_{i,x}, k_{i,y}, k_{i,z})$ to (k_x, k_y, k_z) and its inverse transform $\mathbf{\Gamma}_0^{-1}$, respectively, as

$$(k_x, k_y, k_z)^t = \mathbf{\Gamma}_0 (k_{i,x}, k_{i,y}, k_{i,z})^t = \frac{1}{n}\left(k_{i,x}, k_{i,y}, -\sqrt{n^2 - (1 - k_{i,z}^2)}\right)^t, \tag{5a}$$

$$(k_{i,x}, k_{i,y}, k_{i,z})^t = \mathbf{\Gamma}_0^{-1} (k_x, k_y, k_z)^t = n\left(k_x, k_y, -\sqrt{1 - n^2(1 - k_z^2)}\right)^t. \tag{5b}$$

As is well known, an imperfect corner cube shows a six-beam reflection pattern [2]. If the apex point P_5 deviates from the perfect point, $(\bar{x}_c, \bar{y}_c, -\bar{h})$, the reflection rays are split into six rays, but in the perfect corner cube the six-ray reflection transforms become the same form, and perfect retroreflection occurs. We can count the six possible paths of rays traveling inside the corner cube as (i) $T_0 \to T_1 \to T_2 \to T_3 \to T_0$, (ii) $T_0 \to T_1 \to T_3 \to T_2 \to T_0$, (iii) $T_0 \to T_2 \to T_1 \to T_3 \to T_0$, (iv) $T_0 \to T_2 \to T_3 \to T_1 \to T_0$, (v) $T_0 \to T_3 \to T_2 \to T_1 \to T_0$, and (vi) $T_0 \to T_3 \to T_1 \to T_2 \to T_0$. The six ray traces are represented by the following six transforms:

$$\begin{pmatrix} k_{r,x} \\ k_{r,y} \\ k_{r,z} \end{pmatrix} = \mathbf{\Gamma}_0^{-1}\mathbf{\Gamma}_3\mathbf{\Gamma}_2\mathbf{\Gamma}_1\mathbf{\Gamma}_0 \begin{pmatrix} k_{i,x} \\ k_{i,y} \\ k_{i,z} \end{pmatrix} \quad \text{for } T_0 \to T_1 \to T_2 \to T_3 \to T_0, \tag{6a}$$

$$\begin{pmatrix} k_{r,x} \\ k_{r,y} \\ k_{r,z} \end{pmatrix} = \mathbf{\Gamma}_0^{-1}\mathbf{\Gamma}_2\mathbf{\Gamma}_3\mathbf{\Gamma}_1\mathbf{\Gamma}_0 \begin{pmatrix} k_{i,x} \\ k_{i,y} \\ k_{i,z} \end{pmatrix} \quad \text{for } T_0 \to T_1 \to T_3 \to T_2 \to T_0, \tag{6b}$$

$$\begin{pmatrix} k_{r,x} \\ k_{r,y} \\ k_{r,z} \end{pmatrix} = \mathbf{\Gamma}_0^{-1}\mathbf{\Gamma}_3\mathbf{\Gamma}_1\mathbf{\Gamma}_2\mathbf{\Gamma}_0 \begin{pmatrix} k_{i,x} \\ k_{i,y} \\ k_{i,z} \end{pmatrix} \quad \text{for } T_0 \to T_2 \to T_1 \to T_3 \to T_0, \tag{6c}$$

$$\begin{pmatrix} k_{r,x} \\ k_{r,y} \\ k_{r,z} \end{pmatrix} = \mathbf{\Gamma}_0^{-1}\mathbf{\Gamma}_1\mathbf{\Gamma}_3\mathbf{\Gamma}_2\mathbf{\Gamma}_0 \begin{pmatrix} k_{i,x} \\ k_{i,y} \\ k_{i,z} \end{pmatrix} \quad \text{for } T_0 \to T_2 \to T_3 \to T_1 \to T_0, \tag{6d}$$

$$\begin{pmatrix} k_{r,x} \\ k_{r,y} \\ k_{r,z} \end{pmatrix} = \mathbf{\Gamma}_0^{-1}\mathbf{\Gamma}_1\mathbf{\Gamma}_2\mathbf{\Gamma}_3\mathbf{\Gamma}_0 \begin{pmatrix} k_{i,x} \\ k_{i,y} \\ k_{i,z} \end{pmatrix} \quad \text{for } T_0 \to T_3 \to T_2 \to T_1 \to T_0, \tag{6e}$$

$$\begin{pmatrix} k_{r,x} \\ k_{r,y} \\ k_{r,z} \end{pmatrix} = \mathbf{\Gamma}_0^{-1}\mathbf{\Gamma}_2\mathbf{\Gamma}_1\mathbf{\Gamma}_3\mathbf{\Gamma}_0 \begin{pmatrix} k_{i,x} \\ k_{i,y} \\ k_{i,z} \end{pmatrix} \quad \text{for } T_0 \to T_3 \to T_1 \to T_2 \to T_0. \tag{6f}$$

In Fig. 3, the retroreflection patterns of the corner cube analyzed with the described geometrical optics model is presented. In this simulation, a ray is normally incident on the incidence triangle facet of a single corner cube. With the apex point of the corner cube continuously varied along the spiral spatial traces, the reflection patterns with six reflected rays are continuously recorded on a hemispherical surface. In Figs. 3(a) and 3(c), the blue outlined corner cube is the perfect corner cube structure with $(l_{12}, l_{13}, l_{23}) = (240\,\mu\text{m}, 240\,\mu\text{m}, 240\,\mu\text{m})$ [see Fig. 2(b)]. The spiral traces of the apex point, $P_5(\bar{x}_c + \hat{x}, \bar{y}_c + \hat{y}, -(\bar{h} + \hat{z}))$, of the imperfect corner cube with $\hat{z} > 0$ and $\hat{z} < 0$ are shown in Figs. 3(a) and 3(c), respectively. In Figs. 3(b) and 3(d), the traces of six distinguished reflection rays on the hemispherical surface are plotted, where the rays along the paths, (i) $T_0 \to T_1 \to T_2 \to T_3 \to T_0$, (ii) $T_0 \to T_1 \to T_3 \to T_2 \to T_0$, (iii) $T_0 \to T_2 \to T_1 \to T_3 \to T_0$, (iv) $T_0 \to T_2 \to T_3 \to T_1 \to T_0$, (v) $T_0 \to T_3 \to T_2 \to T_1 \to T_0$, and (vi) $T_0 \to T_3 \to T_1 \to T_2 \to T_0$ are colored red, blue, black, pink, green, and yellow, respectively.

From the theoretical point of view, one can see that combinations of angular errors lead to four possibilities: (i) one-beam reflection (perfect retroreflection), (ii) six-beam reflection (as shown in Fig. 3), (iii) two-beam reflection, and (iv) four-beam reflection. The first and second cases are illustrated in Fig. 3. The third and fourth cases are analyzed further in Appendix C. Although retroreflection by an imperfect corner cube can be classified into the above four categories, the proposed mathematical method to inversely extract the positional error of the apex point of an imperfect retroreflection corner cube is equally applicable to all cases of two-, four-, and six-beam reflections, since two-beam and four-beam reflections are just special cases of six-beam reflection, as is proved in Appendix C.

The reflection transforms are the function of the unknown structural error, $(\hat{x}, \hat{y}, \hat{z})$. Hence, the reflection transforms can be denoted $\mathbf{\Gamma}_i(\hat{x}, \hat{y}, \hat{z})$ $(i = 1, 2, 3)$. As is shown in Fig. 3, for a specific structural error, a corresponding six-beam reflection pattern on the hemispherical surface is measured. Let us separately denote a specific structural error and the unknown structural error variables by $(\hat{x}*, \hat{y}*, \hat{z}*)$ and $(\hat{x}, \hat{y}, \hat{z})$, respectively. Then, we can interpret six reflection transforms $\mathbf{A}_i$ $(i = 1, 2, \ldots, 6)$ from the reflection pattern, which take the form of combinatorial multiplication of three facet reflection transforms as

$$\mathbf{A}_1 = \mathbf{\Gamma}_3(\hat{x}*, \hat{y}*, \hat{z}*)\mathbf{\Gamma}_2(\hat{x}*, \hat{y}*, \hat{z}*)\mathbf{\Gamma}_1(\hat{x}*, \hat{y}*, \hat{z}*), \tag{7a}$$

$$\mathbf{A}_2 = \mathbf{\Gamma}_2(\hat{x}*, \hat{y}*, \hat{z}*)\mathbf{\Gamma}_3(\hat{x}*, \hat{y}*, \hat{z}*)\mathbf{\Gamma}_1(\hat{x}*, \hat{y}*, \hat{z}*), \tag{7b}$$

$$\mathbf{A}_3 = \mathbf{\Gamma}_3(\hat{x}*, \hat{y}*, \hat{z}*)\mathbf{\Gamma}_1(\hat{x}*, \hat{y}*, \hat{z}*)\mathbf{\Gamma}_2(\hat{x}*, \hat{y}*, \hat{z}*), \tag{7c}$$

$$\mathbf{A}_4 = \mathbf{\Gamma}_1(\hat{x}*, \hat{y}*, \hat{z}*)\mathbf{\Gamma}_3(\hat{x}*, \hat{y}*, \hat{z}*)\mathbf{\Gamma}_2(\hat{x}*, \hat{y}*, \hat{z}*), \tag{7d}$$

$$\mathbf{A}_5 = \mathbf{\Gamma}_1(\hat{x}*, \hat{y}*, \hat{z}*)\mathbf{\Gamma}_2(\hat{x}*, \hat{y}*, \hat{z}*)\mathbf{\Gamma}_3(\hat{x}*, \hat{y}*, \hat{z}*), \tag{7e}$$

$$\mathbf{A}_6 = \mathbf{\Gamma}_2(\hat{x}*, \hat{y}*, \hat{z}*)\mathbf{\Gamma}_1(\hat{x}*, \hat{y}*, \hat{z}*)\mathbf{\Gamma}_3(\hat{x}*, \hat{y}*, \hat{z}*). \tag{7f}$$

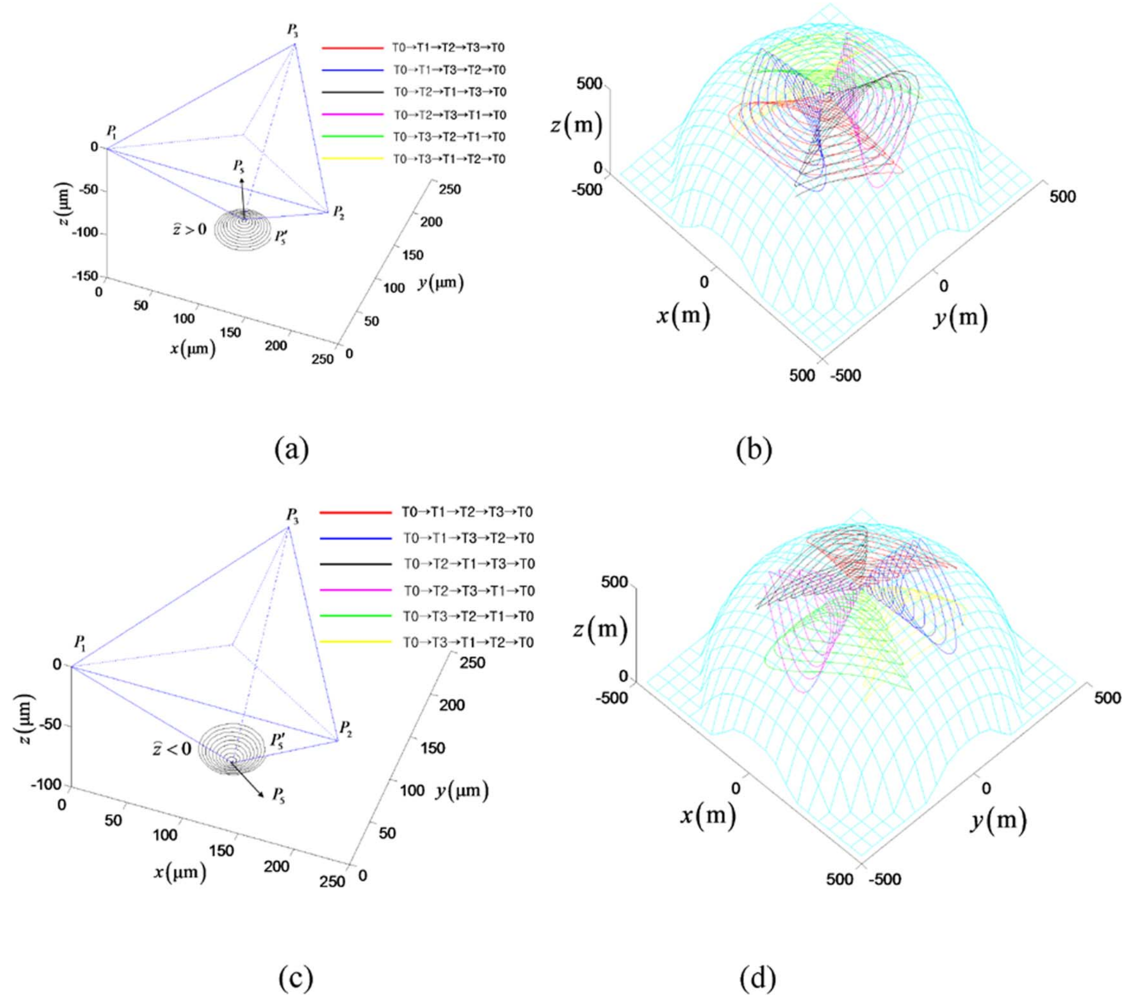

Fig. 3. (Color online) (a) Trace of the apex point $P_5(\hat{z} > 0)$ of an imperfect corner cube; (b) traces of six distinguished reflection rays on the hemispherical surface; (c) a trace of the apex point $P_5(\hat{z} < 0)$ of an imperfect corner cube; (d) traces of six distinguished reflection rays on the hemispherical surface.

The reflection transform data, $\mathbf{A}_1$, $\mathbf{A}_2$, $\mathbf{A}_3$, $\mathbf{A}_4$, $\mathbf{A}_5$, and $\mathbf{A}_6$, are optically measurable data for a specific imperfect corner cube with the structural error $(\hat{x}*, \hat{y}*, \hat{z}*)$. By measuring the continuous trace of the reflection pattern with the incidence light directions varying, we can measure the reflection transforms $\mathbf{A}_i$ $(i = 1, 2, \ldots, 6)$. Once these data are obtained, we can further proceed to extract the structural error $(\hat{x}*, \hat{y}*, \hat{z}*)$ implicitly imbedded in the six reflection transform data from the measured data. The first reflection transform of Eq. (6a) is slightly modified, from Eq. (7a), as

$$\mathbf{\Gamma}_0 \begin{pmatrix} k_{r,x} \\ k_{r,y} \\ k_{r,z} \end{pmatrix} = \mathbf{A}_1 \mathbf{\Gamma}_0 \begin{pmatrix} k_{i,x} \\ k_{i,y} \\ k_{i,z} \end{pmatrix}. \tag{8a}$$

For the direction vectors of several incidence rays, $(k_{i,x}^{(1)}, k_{i,y}^{(1)}, k_{i,z}^{(1)}), \ldots, (k_{i,x}^{(M)}, k_{i,y}^{(M)}, k_{i,z}^{(M)})$, we can measure the reflection ray vectors $(k_{r,x}^{(1)}, k_{r,y}^{(1)}, k_{r,z}^{(1)}), \ldots, (k_{r,x}^{(M)}, k_{r,y}^{(M)}, k_{r,z}^{(M)})$ with $M \geq 3$. From Eq. (8a), the measured data are arranged as

$$\mathbf{\Gamma}_0 \begin{pmatrix} k_{r,x}^{(1)} & k_{r,x}^{(2)} & \ldots & k_{r,x}^{(M-1)} & k_{r,x}^{(M)} \\ k_{r,y}^{(1)} & k_{r,y}^{(2)} & \ldots & k_{r,y}^{(M-1)} & k_{r,y}^{(M)} \\ k_{r,z}^{(1)} & k_{r,z}^{(2)} & \ldots & k_{r,z}^{(M-1)} & k_{r,z}^{(M)} \end{pmatrix} = \mathbf{A}_1 \mathbf{\Gamma}_0 \begin{pmatrix} k_{i,x}^{(1)} & k_{i,x}^{(2)} & \ldots & k_{i,x}^{(M-1)} & k_{i,x}^{(M)} \\ k_{i,y}^{(1)} & k_{i,y}^{(2)} & \ldots & k_{i,y}^{(M-1)} & k_{i,y}^{(M)} \\ k_{i,z}^{(1)} & k_{i,z}^{(2)} & \ldots & k_{i,z}^{(M-1)} & k_{i,z}^{(M)} \end{pmatrix}. \tag{8b}$$

Because the nonlinear refraction transform $\mathbf{\Gamma}_0$ is explicitly known, we can obtain $\mathbf{A}_1$ by using the linear least squares method [24,25]. According to the linear least squares method, the solution of Eq. (8b), $\mathbf{A}_1$, is represented by

$$\mathbf{A}_1 = \mathbf{R}\mathbf{C}^t(\mathbf{C}\mathbf{C}^t)^{-1}, \tag{8c}$$

where $\mathbf{R}$ and $\mathbf{C}$ are defined, respectively, by

$$\mathbf{R} = \mathbf{\Gamma}_0 \begin{pmatrix} k_{r,x}^{(1)} & k_{r,x}^{(2)} & \ldots & k_{r,x}^{(M-1)} & k_{r,x}^{(M)} \\ k_{r,y}^{(1)} & k_{r,y}^{(2)} & \ldots & k_{r,y}^{(M-1)} & k_{r,y}^{(M)} \\ k_{r,z}^{(1)} & k_{r,z}^{(2)} & \ldots & k_{r,z}^{(M-1)} & k_{r,z}^{(M)} \end{pmatrix}, \tag{9a}$$

$$\mathbf{C} = \mathbf{\Gamma}_0 \begin{pmatrix} k_{i,x}^{(1)} & k_{i,x}^{(2)} & \ldots & k_{i,x}^{(M-1)} & k_{i,x}^{(M)} \\ k_{i,y}^{(1)} & k_{i,y}^{(2)} & \ldots & k_{i,y}^{(M-1)} & k_{i,y}^{(M)} \\ k_{i,z}^{(1)} & k_{i,z}^{(2)} & \ldots & k_{i,z}^{(M-1)} & k_{i,z}^{(M)} \end{pmatrix}. \tag{9b}$$

By the optical measurement of the reflection patterns, we can know all six reflection transforms, $\mathbf{A}_1$, $\mathbf{A}_2$, $\mathbf{A}_3$, $\mathbf{A}_4$, $\mathbf{A}_5$, and $\mathbf{A}_6$, for a specific structural error $(\hat{x}*, \hat{y}*, \hat{z}*)$ with the structural error itself being unknown. However, it should be noted that, in the measurement, we have just six reflection transforms without identifying the correspondence of each of the six reflection transforms to its own ray path.

3. Structural Analysis of a Single Corner Cube by the Nonlinear Conjugate Gradient Method

The heart of this paper is the inverse analysis of extracting the structural error of the examined corner cube from the optically measurable data, $\mathbf{A}_i$ $(i = 1, 2, \ldots, 6)$. In this section, the numerical method of structural error extraction from the optically measurable data, $\mathbf{A}_i$ $(i = 1, 2, \ldots, 6)$ is elucidated.

The first consideration in the inverse analysis problem is the number of combinatorial cases in the classification of the six measurable data. As stated in the previous section, we have six reflection transforms without identifying the correspondence of each of the six reflection transforms to its own ray path. Therefore, we have total possible combination number of 720 $(= 6!)$ with respect to matching the measured data to the six ray traces of the examined imperfect corner cube. Hence, the inevitable step in the inverse structural analysis is that we have to find the best-matched one among all possible 720 combination cases.

Let us consider the set of six retroreflection paths parameterized by $(\hat{x}, \hat{y}, \hat{z})$, given by $\{\mathbf{\Gamma}_3\mathbf{\Gamma}_2\mathbf{\Gamma}_1, \mathbf{\Gamma}_2\mathbf{\Gamma}_3\mathbf{\Gamma}_1, \mathbf{\Gamma}_3\mathbf{\Gamma}_1\mathbf{\Gamma}_2, \mathbf{\Gamma}_1\mathbf{\Gamma}_3\mathbf{\Gamma}_2, \mathbf{\Gamma}_1\mathbf{\Gamma}_2\mathbf{\Gamma}_3, \mathbf{\Gamma}_2\mathbf{\Gamma}_1\mathbf{\Gamma}_3\}$. The error function parameterized by $(\hat{x}, \hat{y}, \hat{z})$, $E(\hat{x}, \hat{y}, \hat{z})$, that measures the amount of the error of the reflection characteristics of the corner cube from that of the inspected corner cube with the structural parameters $(\hat{x}*, \hat{y}*, \hat{z}*)$ is defined by

$$\begin{aligned} E(\hat{x}, \hat{y}, \hat{z}) = {} & |\mathbf{A}_{n_1} - \mathbf{\Gamma}_3\mathbf{\Gamma}_2\mathbf{\Gamma}_1|^2 + |\mathbf{A}_{n_2} - \mathbf{\Gamma}_2\mathbf{\Gamma}_3\mathbf{\Gamma}_1|^2 \\ & + |\mathbf{A}_{n_3} - \mathbf{\Gamma}_3\mathbf{\Gamma}_1\mathbf{\Gamma}_2|^2 + |\mathbf{A}_{n_4} - \mathbf{\Gamma}_1\mathbf{\Gamma}_3\mathbf{\Gamma}_2|^2 \\ & + |\mathbf{A}_{n_5} - \mathbf{\Gamma}_1\mathbf{\Gamma}_2\mathbf{\Gamma}_3|^2 + |\mathbf{A}_{n_6} - \mathbf{\Gamma}_2\mathbf{\Gamma}_1\mathbf{\Gamma}_3|^2, \end{aligned} \tag{10a}$$

where the absolute value symbol $|\mathbf{A}|^2$ is defined as the sum of squared values of all elements of $\mathbf{A}$ as

$$\begin{aligned} |\mathbf{A}|^2 = {} & a_{11}^2 + a_{12}^2 + a_{13}^2 + a_{21}^2 + a_{22}^2 + a_{23}^2 \\ & + a_{31}^2 + a_{32}^2 + a_{33}^2 \end{aligned} \tag{10b}$$

and the index pair $(n_1, n_2, n_3, n_4, n_5, n_6)$ indicates a possible index pair among total 720 combinations. Then we should separately inspect a total of 720 error functions and find the optimal variables $(\hat{x}, \hat{y}, \hat{z})$ minimizing the error function for each combination. In the analysis stage, for example, the cases $(n_1, n_2, n_3, n_4, n_5, n_6) = (1, 2, 3, 4, 5, 6)$ and $(n_1, n_2, n_3, n_4, n_5, n_6) = (3, 5, 4, 6, 1, 2)$ are inspected with the same possibility of 1/720, because we do not have *a priori* information on the matching of the measurable data, $\mathbf{A}_1, \mathbf{A}_2, \mathbf{A}_3, \mathbf{A}_4, \mathbf{A}_5$, and $\mathbf{A}_6$ to respective retroreflection paths. Hence, after obtaining the minimizing variables $(\hat{x}, \hat{y}, \hat{z})$ of all 720 cases, we should select the case showing the minimum-error function value among 720 cases, and we can identify the value $(\hat{x}, \hat{y}, \hat{z})$ at this case with the approximate solution to the true structural factor $(\hat{x}*, \hat{y}*, \hat{z}*)$.

The structural error extraction is formulated as a nonlinear optimization problem for solving the minimal condition of Eq. (10a). In this paper, the NCGM is employed to solve the posed nonlinear optimization problem, and its detailed formulation is developed. In the standard NCGM, minimization of the objective function is performed by consecutive iterative procedures [24]. The core in the NCGM is the calculation of the gradient vector, $\nabla E(\hat{x}, \hat{y}, \hat{z})$, of the objective function $E(\hat{x}, \hat{y}, \hat{z})$. The gradient vector takes the form

$$\nabla E(\hat{x}, \hat{y}, \hat{z}) = [\partial_{\hat{x}} E(\hat{x}, \hat{y}, \hat{z}), \partial_{\hat{y}} E(\hat{x}, \hat{y}, \hat{z}), \partial_{\hat{z}} E(\hat{x}, \hat{y}, \hat{z})]. \tag{11}$$

Before expressing the explicit form of Eq. (11), let us obtain the total derivative of $E(\hat{x}, \hat{y}, \hat{z})$. The total derivative, $\Delta E(\hat{x}, \hat{y}, \hat{z})$, is represented by the form

$$\begin{aligned} \Delta E(\hat{x}, \hat{y}, \hat{z}) = {} & [\![(\mathbf{A}_{n_1} - \mathbf{\Gamma}_3\mathbf{\Gamma}_2\mathbf{\Gamma}_1) \odot (-2\Delta(\mathbf{\Gamma}_3\mathbf{\Gamma}_2\mathbf{\Gamma}_1))]\!] \\ & + [\![(\mathbf{A}_{n_2} - \mathbf{\Gamma}_2\mathbf{\Gamma}_3\mathbf{\Gamma}_1) \odot (-2\Delta(\mathbf{\Gamma}_2\mathbf{\Gamma}_3\mathbf{\Gamma}_1))]\!] \\ & + [\![(\mathbf{A}_{n_3} - \mathbf{\Gamma}_3\mathbf{\Gamma}_1\mathbf{\Gamma}_2) \odot (-2\Delta(\mathbf{\Gamma}_3\mathbf{\Gamma}_1\mathbf{\Gamma}_2))]\!] \\ & + [\![(\mathbf{A}_{n_4} - \mathbf{\Gamma}_1\mathbf{\Gamma}_3\mathbf{\Gamma}_2) \odot (-2\Delta(\mathbf{\Gamma}_1\mathbf{\Gamma}_3\mathbf{\Gamma}_2))]\!] \\ & + [\![(\mathbf{A}_{n_5} - \mathbf{\Gamma}_1\mathbf{\Gamma}_2\mathbf{\Gamma}_3) \odot (-2\Delta(\mathbf{\Gamma}_1\mathbf{\Gamma}_2\mathbf{\Gamma}_3))]\!] \\ & + [\![(\mathbf{A}_{n_6} - \mathbf{\Gamma}_2\mathbf{\Gamma}_1\mathbf{\Gamma}_3) \odot (-2\Delta(\mathbf{\Gamma}_2\mathbf{\Gamma}_1\mathbf{\Gamma}_3))]\!], \end{aligned} \tag{12a}$$

where $\mathbf{A} \odot \mathbf{B}$ is the entry-by-entry product of $\mathbf{A}$ and $\mathbf{B}$. Here $\mathbf{A}$ and $\mathbf{B}$ are 3×3 matrices. Thus

$$\begin{aligned} \mathbf{A} \odot \mathbf{B} &= \begin{pmatrix} a_{11} & a_{12} & a_{13} \\ a_{21} & a_{22} & a_{23} \\ a_{31} & a_{32} & a_{33} \end{pmatrix} \odot \begin{pmatrix} b_{11} & b_{12} & b_{13} \\ b_{21} & b_{22} & b_{23} \\ b_{31} & b_{32} & b_{33} \end{pmatrix} \\ &= \begin{pmatrix} a_{11}b_{11} & a_{12}b_{12} & a_{13}b_{13} \\ a_{21}b_{21} & a_{22}b_{22} & a_{23}b_{23} \\ a_{31}b_{31} & a_{32}b_{32} & a_{33}b_{33} \end{pmatrix}, \end{aligned} \tag{12b}$$

and $[\![\mathbf{A}]\!]$ is the sum of all elements of $\mathbf{A}$,

$$[\![\mathbf{A}]\!] = a_{11} + a_{12} + a_{13} + a_{21} + a_{22} + a_{23} + a_{31} + a_{32} + a_{33}. \tag{12c}$$

The elements of the gradient vector $\nabla E(\hat{x},\hat{y},\hat{z})$ are obtained from the total derivative, Eq. (12a), respectively, as

$$\begin{aligned}\partial_{\hat{x}} E(\hat{x},\hat{y},\hat{z}) &= \lim_{\Delta\hat{x}\to 0} \Delta E(\hat{x},\hat{y},\hat{z})/\Delta\hat{x} \\ &= [\![(\mathbf{A}_1 - \mathbf{\Gamma}_3\mathbf{\Gamma}_2\mathbf{\Gamma}_1)\odot(-2\partial_{\hat{x}}(\mathbf{\Gamma}_3\mathbf{\Gamma}_2\mathbf{\Gamma}_1))]\!] \\ &\quad + [\![(\mathbf{A}_2 - \mathbf{\Gamma}_2\mathbf{\Gamma}_3\mathbf{\Gamma}_1)\odot(-2\partial_{\hat{x}}(\mathbf{\Gamma}_2\mathbf{\Gamma}_3\mathbf{\Gamma}_1))]\!] \\ &\quad + [\![(\mathbf{A}_3 - \mathbf{\Gamma}_3\mathbf{\Gamma}_1\mathbf{\Gamma}_2)\odot(-2\partial_{\hat{x}}(\mathbf{\Gamma}_3\Gamma_1\mathbf{\Gamma}_2))]\!] \\ &\quad + [\![(\mathbf{A}_4 - \mathbf{\Gamma}_1\mathbf{\Gamma}_3\mathbf{\Gamma}_2)\odot(-2\partial_{\hat{x}}(\mathbf{\Gamma}_1\Gamma_3\mathbf{\Gamma}_2))]\!] \\ &\quad + [\![(\mathbf{A}_5 - \mathbf{\Gamma}_1\mathbf{\Gamma}_2\mathbf{\Gamma}_3)\odot(-2\partial_{\hat{x}}(\mathbf{\Gamma}_1\Gamma_2\mathbf{\Gamma}_3))]\!] \\ &\quad + [\![(\mathbf{A}_6 - \mathbf{\Gamma}_2\mathbf{\Gamma}_1\mathbf{\Gamma}_3)\odot(-2\partial_{\hat{x}}(\mathbf{\Gamma}_2\mathbf{\Gamma}_1\mathbf{\Gamma}_3))]\!],\end{aligned} \tag{13a}$$

$$\begin{aligned}\partial_{\hat{y}} E(\hat{x},\hat{y},\hat{z}) &= \lim_{\Delta\hat{y}\to 0} \Delta E(\hat{x},\hat{y},\hat{z})/\Delta\hat{y} \\ &= [\![(\mathbf{A}_1 - \mathbf{\Gamma}_3\mathbf{\Gamma}_2\mathbf{\Gamma}_1)\odot(-2\partial_{\hat{y}}(\mathbf{\Gamma}_3\mathbf{\Gamma}_2\mathbf{\Gamma}_1))]\!] \\ &\quad + [\![(\mathbf{A}_2 - \mathbf{\Gamma}_2\mathbf{\Gamma}_3\mathbf{\Gamma}_1)\odot(-2\partial_{\hat{y}}(\mathbf{\Gamma}_2\mathbf{\Gamma}_3\mathbf{\Gamma}_1))]\!] \\ &\quad + [\![(\mathbf{A}_3 - \mathbf{\Gamma}_3\mathbf{\Gamma}_1\mathbf{\Gamma}_2)\odot(-2\partial_{\hat{y}}(\mathbf{\Gamma}_3\mathbf{\Gamma}_1\mathbf{\Gamma}_2))]\!] \\ &\quad + [\![(\mathbf{A}_4 - \mathbf{\Gamma}_1\mathbf{\Gamma}_3\mathbf{\Gamma}_2)\odot(-2\partial_{\hat{y}}(\mathbf{\Gamma}_1\mathbf{\Gamma}_3\mathbf{\Gamma}_2))]\!] \\ &\quad + [\![(\mathbf{A}_5 - \mathbf{\Gamma}_1\mathbf{\Gamma}_2\mathbf{\Gamma}_3)\odot(-2\partial_{\hat{y}}(\mathbf{\Gamma}_1\mathbf{\Gamma}_2\mathbf{\Gamma}_3))]\!] \\ &\quad + [\![(\mathbf{A}_6 - \mathbf{\Gamma}_2\mathbf{\Gamma}_1\mathbf{\Gamma}_3)\odot(-2\partial_{\hat{y}}(\mathbf{\Gamma}_2\mathbf{\Gamma}_1\mathbf{\Gamma}_3))]\!],\end{aligned} \tag{13b}$$

$$\begin{aligned}\partial_{\hat{z}} E(\hat{x},\hat{y},\hat{z}) &= \lim_{\Delta\hat{z}\to 0} \Delta E(\hat{x},\hat{y},\hat{z})/\Delta\hat{z} \\ &= [\![(\mathbf{A}_1 - \mathbf{\Gamma}_3\mathbf{\Gamma}_2\mathbf{\Gamma}_1)\odot(-2\partial_{\hat{z}}(\mathbf{\Gamma}_3\mathbf{\Gamma}_2\mathbf{\Gamma}_1))]\!] \\ &\quad + [\![(\mathbf{A}_2 - \mathbf{\Gamma}_2\mathbf{\Gamma}_3\mathbf{\Gamma}_1)\odot(-2\partial_{\hat{z}}(\mathbf{\Gamma}_2\Gamma_3\mathbf{\Gamma}_1))]\!] \\ &\quad + [\![(\mathbf{A}_3 - \mathbf{\Gamma}_3\mathbf{\Gamma}_1\mathbf{\Gamma}_2)\odot(-2\partial_{\hat{z}}(\mathbf{\Gamma}_3\mathbf{\Gamma}_1\mathbf{\Gamma}_2))]\!] \\ &\quad + [\![(\mathbf{A}_4 - \mathbf{\Gamma}_1\mathbf{\Gamma}_3\mathbf{\Gamma}_2)\odot(-2\partial_{\hat{z}}(\mathbf{\Gamma}_1\mathbf{\Gamma}_3\mathbf{\Gamma}_2))]\!] \\ &\quad + [\![(\mathbf{A}_5 - \mathbf{\Gamma}_1\mathbf{\Gamma}_2\mathbf{\Gamma}_3)\odot(-2\partial_{\hat{z}}(\mathbf{\Gamma}_1\mathbf{\Gamma}_2\mathbf{\Gamma}_3))]\!] \\ &\quad + [\![(\mathbf{A}_6 - \mathbf{\Gamma}_2\mathbf{\Gamma}_1\mathbf{\Gamma}_3)\odot(-2\partial_{\hat{z}}(\mathbf{\Gamma}_2\mathbf{\Gamma}_1\mathbf{\Gamma}_3))]\!],\end{aligned} \tag{13c}$$

where the partial derivatives, $\partial_{\hat{x}(\hat{y},\hat{z})}(\mathbf{\Gamma}_3\mathbf{\Gamma}_2\mathbf{\Gamma}_1)$, $\partial_{\hat{x}(\hat{y},\hat{z})}(\mathbf{\Gamma}_2\mathbf{\Gamma}_3\mathbf{\Gamma}_1)$, $\partial_{\hat{x}(\hat{y},\hat{z})}(\mathbf{\Gamma}_3\mathbf{\Gamma}_1\mathbf{\Gamma}_2)$, $\partial_{\hat{x}(\hat{y},\hat{z})}(\mathbf{\Gamma}_1\mathbf{\Gamma}_3\mathbf{\Gamma}_2)$, $\partial_{\hat{x}(\hat{y},\hat{z})}(\mathbf{\Gamma}_1\mathbf{\Gamma}_2\mathbf{\Gamma}_3)$, and $\partial_{\hat{x}(\hat{y},\hat{z})}(\mathbf{\Gamma}_2\mathbf{\Gamma}_1\mathbf{\Gamma}_3)$ are derived as

$$\partial_{\hat{x}(\hat{y},\hat{z})}(\mathbf{\Gamma}_3\mathbf{\Gamma}_2\mathbf{\Gamma}_1) = \partial_{\hat{x}(\hat{y},\hat{z})}\mathbf{\Gamma}_3\mathbf{\Gamma}_2\mathbf{\Gamma}_1 + \mathbf{\Gamma}_3\partial_{\hat{x}(\hat{y},\hat{z})}\mathbf{\Gamma}_2\mathbf{\Gamma}_1 + \mathbf{\Gamma}_3\mathbf{\Gamma}_2\partial_{\hat{x}(\hat{y},\hat{z})}\mathbf{\Gamma}_1, \tag{14a}$$

$$\partial_{\hat{x}(\hat{y},\hat{z})}(\mathbf{\Gamma}_2\mathbf{\Gamma}_3\mathbf{\Gamma}_1) = \partial_{\hat{x}(\hat{y},\hat{z})}\mathbf{\Gamma}_2\mathbf{\Gamma}_3\mathbf{\Gamma}_1 + \mathbf{\Gamma}_2\partial_{\hat{x}(\hat{y},\hat{z})}\mathbf{\Gamma}_3\mathbf{\Gamma}_1 + \mathbf{\Gamma}_2\mathbf{\Gamma}_3\partial_{\hat{x}(\hat{y},\hat{z})}\mathbf{\Gamma}_1, \tag{14b}$$

$$\partial_{\hat{x}(\hat{y},\hat{z})}(\mathbf{\Gamma}_3\mathbf{\Gamma}_1\mathbf{\Gamma}_2) = \partial_{\hat{x}(\hat{y},\hat{z})}\mathbf{\Gamma}_3\mathbf{\Gamma}_1\mathbf{\Gamma}_2 + \mathbf{\Gamma}_3\partial_{\hat{x}(\hat{y},\hat{z})}\mathbf{\Gamma}_1\mathbf{\Gamma}_2 + \mathbf{\Gamma}_3\mathbf{\Gamma}_1\partial_{\hat{x}(\hat{y},\hat{z})}\mathbf{\Gamma}_2, \tag{14c}$$

$$\partial_{\hat{x}(\hat{y},\hat{z})}(\mathbf{\Gamma}_1\mathbf{\Gamma}_3\mathbf{\Gamma}_2) = \partial_{\hat{x}(\hat{y},\hat{z})}\mathbf{\Gamma}_1\mathbf{\Gamma}_3\mathbf{\Gamma}_2 + \mathbf{\Gamma}_1\partial_{\hat{x}(\hat{y},\hat{z})}\mathbf{\Gamma}_3\mathbf{\Gamma}_2 + \mathbf{\Gamma}_1\mathbf{\Gamma}_3\partial_{\hat{x}(\hat{y},\hat{z})}\mathbf{\Gamma}_2, \tag{14d}$$

$$\partial_{\hat{x}(\hat{y},\hat{z})}(\mathbf{\Gamma}_1\mathbf{\Gamma}_2\mathbf{\Gamma}_3) = \partial_{\hat{x}(\hat{y},\hat{z})}\mathbf{\Gamma}_1\mathbf{\Gamma}_2\mathbf{\Gamma}_3 + \mathbf{\Gamma}_1\partial_{\hat{x}(\hat{y},\hat{z})}\mathbf{\Gamma}_2\mathbf{\Gamma}_3 + \mathbf{\Gamma}_1\mathbf{\Gamma}_2\partial_{\hat{x}(\hat{y},\hat{z})}\mathbf{\Gamma}_3, \tag{14e}$$

$$\partial_{\hat{x}(\hat{y},\hat{z})}(\mathbf{\Gamma}_2\mathbf{\Gamma}_1\mathbf{\Gamma}_3) = \partial_{\hat{x}(\hat{y},\hat{z})}\mathbf{\Gamma}_2\mathbf{\Gamma}_1\mathbf{\Gamma}_3 + \mathbf{\Gamma}_2\partial_{\hat{x}(\hat{y},\hat{z})}\mathbf{\Gamma}_1\mathbf{\Gamma}_3 + \mathbf{\Gamma}_2\mathbf{\Gamma}_1\partial_{\hat{x}(\hat{y},\hat{z})}\mathbf{\Gamma}_3. \tag{14f}$$

The partial derivatives $\partial_{\hat{x}(\hat{y},\hat{z})}\mathbf{\Gamma}_1$, $\partial_{\hat{x}(\hat{y},\hat{z})}\mathbf{\Gamma}_2$, and $\partial_{\hat{x}(\hat{y},\hat{z})}\mathbf{\Gamma}_3$ are detailed in Appendix D. In the standard NCGM, the structural error $(\hat{x}_m,\hat{y}_m,\hat{z}_m)$ can be obtained through the convergence of an iteration procedure. The structural error at the $(m+1)$th iteration stage, $(\hat{x}_{m+1},\hat{y}_{m+1},\hat{z}_{m+1})$, is updated from the structural error at the mth iteration stage, $(\hat{x}_m,\hat{y}_m,\hat{z}_m)$, through the formula

$$(\hat{x}_{m+1},\hat{y}_{m+1},\hat{z}_{m+1}) = (\hat{x}_m,\hat{y}_m,\hat{z}_m) + \tau_m\mathbf{d}_m \quad \text{for } m = 0,1,2,\ldots, \tag{15}$$

where τ_m and $\mathbf{d}_m$ denote the step size and the search direction vector, respectively, at the $(m+1)$th iteration stage. The search direction vector $\mathbf{d}_m$ is given by

$$\mathbf{d}_m = -\nabla E(\hat{x}_m,\hat{y}_m,\hat{z}_m) + \beta_{m-1}\mathbf{d}_{m-1}, \tag{16}$$

where the Fletcher–Reeves formula [24] sets β_{m-1} to

$$\beta_{m-1} = \frac{|\nabla E(\hat{x}_m,\hat{y}_m,\hat{z}_m)|^2}{|\nabla E(\hat{x}_{m-1},\hat{y}_{m-1},\hat{z}_{m-1})|^2}. \tag{17}$$

The step size τ_m is determined in order to minimize the objective function $E(\hat{x}_m,\hat{y}_m,\hat{z}_m)$ with the aid of the bracketing algorithm and the golden section search algorithm [25]. In the analysis, the initial value of the structural error $(\hat{x}_0,\hat{y}_0,\hat{z}_0)$ is set to $(0,0,0)$. From the structural point of view, the initial point of the NCGM is the perfect corner cube. Through the NCGM iteration procedure, the perfect corner cube at the initial stage evolves to the imperfect corner cube.

We compare two examples of the structural analysis of the imperfect corner cubes with different structural errors. In Figs. 4 and 5 examples of structural error extraction with the NCGM for the relatively large error $(\hat{x}*,\hat{y}*,\hat{z}*) = (12\,\mu\text{m},\ 13\,\mu\text{m},\ 10\,\mu\text{m})$ and the relatively small error, $(\hat{x}*,\hat{y}*,\hat{z}*) = (2\,\mu\text{m},\ 1.5\,\mu\text{m},\ 1\,\mu\text{m})$, are presented, respectively. In Fig. 4(a), the error function values at the 100th iteration stage, $E(\hat{x}_{100},\hat{y}_{100},\hat{z}_{100})$, for the unsorted combination indices are plotted. The combination indexes, 1, 2, 3, 4, …720 in Fig. 4(a) correspond to the consecutive permutation pairs $(n_1,n_2,n_3,n_4,n_5,n_6) = (1,2,3,4,5,6)$, $(n_1,n_2,n_3,n_4,n_5,n_6) = (1,2,3,4,6,5)$, $(n_1,n_2,n_3,n_4,n_5,n_6) = (1,2,3,5,4,6)$, $(n_1,n_2,n_3,n_4,n_5,n_6) = (1,2,3,5,6,4),\ldots,(n_1,n_2,n_3,n_4,n_5,n_6) = (6,5,4,3,2,1)$, respectively. In Fig. 4(b), the sorted error function values are plotted, where the 720 cases are sorted according to the increasing order of the value of $E(\hat{x}_{100},\hat{y}_{100},\hat{z}_{100})$. We can say that the minimum first case, $(n_1,n_2,n_3,n_4,n_5,n_6) = (1,2,3,4,5,6)$, in the sorted result of Fig. 4(b) is the solution of the optimization problem. In Figs. 4(c)–4(e), the convergence curves of $\hat{x}_m$, $\hat{y}_m$, and $\hat{z}_m$ for the combination cases of $(n_1,n_2,n_3,n_4,n_5,n_6) = (1,2,3,4,5,6)$, $(n_1,n_2,n_3,n_4,n_5,n_6) = (5,4,6,2,1,3)$, and $(n_1,n_2,n_3,n_4,n_5,n_6) = (2,4,5,6,3,1)$ that are indicated, respectively, by solid, dashed, and dotted curves are presented. The first case of $(n_1,n_2,n_3,n_4,n_5,n_6) = (1,2,3,4,5,6)$ shows the convergence of $(\hat{x}_{100},\hat{y}_{100},\hat{z}_{100})$ to the structural error $(\hat{x}*,\hat{y}*,\hat{z}*)$. The other two cases of $(n_1,n_2,n_3,n_4,n_5,n_6) = (5,4,6,2,1,3)$ and $(n_1,n_2,n_3,n_4,n_5,n_6) = (2,4,5,6,3,1)$ show the convergence of $(\hat{x}_{100},\hat{y}_{100},\hat{z}_{100})$ to the wrong values $(-12.98\,\mu\text{m},-11.3\,\mu\text{m},-10.6\,\mu\text{m})$ and $(-3.14\,\mu\text{m},-18.59\,\mu\text{m},-5.46\,\mu\text{m})$, respectively. In Fig. 4(f), the convergence curves of $E(\hat{x}_m,\hat{y}_m,\hat{z}_m)$ for the combination cases of $(n_1,n_2,n_3,n_4,n_5,n_6) = (1,2,3,4,5,6)$, $(n_1,n_2,n_3,n_4,n_5,n_6) = (5,4,6,2,1,3)$, and $(n_1,n_2,n_3,n_4,n_5,n_6) = (2,4,5,6,3,1)$ that are also indicated, respectively, by solid, dashed, and dotted curves are presented. As shown in Fig. 4(f), the value of $E(\hat{x}_m,\hat{y}_m,\hat{z}_m)$ of the combination case of $(n_1,n_2,n_3,n_4,n_5,n_6) = (1,2,3,4,5,6)$ goes to zero monotonically.

In Fig. 5, the structural analysis result of the imperfect corner cube with the structural error $(\hat{x}*,\hat{y}*,\hat{z}*) = (2\,\mu\text{m},1.5\,\mu\text{m},1\,\mu\text{m})$ is presented. Figure 5(a) shows the error function values at the 100th iteration stage, $E(\hat{x}_{100},\hat{y}_{100},\hat{z}_{100})$ for the unsorted combination indices. If the cases are sorted according to the increasing order of the value of $E(\hat{x}_{100},\hat{y}_{100},\hat{z}_{100})$, we can find the solution of the optimization problem in the minimum first case in the plot as shown in Fig. 5(b), where the minimum first case is $(n_1,n_2,n_3,n_4,n_5,n_6) = (1,2,3,4,5,6)$. In Figs. 5(c)–5(e), the convergence curves of $\hat{x}_m$, $\hat{y}_m$, and $\hat{z}_m$ for the combination cases of $(n_1,n_2,n_3,n_4,n_5,n_6) = (1,2,3,4,5,6)$, $(n_1,n_2,n_3,n_4,n_5,n_6) = (5,4,6,2,1,3)$, and $(n_1,n_2,n_3,n_4,n_5,n_6) = (2,4,5,6,3,1)$ are indicated, respectively, by solid, dashed, and dotted curves. The first case of $(n_1,n_2,n_3,n_4,n_5,n_6) = (1,2,3,4,5,6)$ shows a good convergence of $(\hat{x}_{100},\hat{y}_{100},\hat{z}_{100})$ to the structural error $(\hat{x}*,\hat{y}*,\hat{z}*)$. The other two cases of $(n_1,n_2,n_3,n_4,n_5,n_6) = (5,4,6,2,1,3)$ and $(n_1,n_2,n_3,n_4,n_5,n_6) = (2,4,5,6,3,1)$ show the convergence of $(\hat{x}_{100},\hat{y}_{100},\hat{z}_{100})$ to the wrong values $(-2.27\,\mu\text{m},-1.4\,\mu\text{m},-1\,\mu\text{m})$ and $(-1.069\,\mu\text{m},-2\,\mu\text{m},-0.64\,\mu\text{m})$, respectively. In Fig. 5(f), the convergence curves of $E(\hat{x}_m,\hat{y}_m,\hat{z}_m)$ for the combination cases of $(n_1,n_2,n_3,n_4,n_5,n_6) = (1,2,3,4,5,6)$, $(n_1,n_2,n_3,n_4,n_5,n_6) = (5,4,6,2,1,3)$, and $(n_1,n_2,n_3,n_4,n_5,n_6) = (2,4,5,6,3,1)$ are indicated, respectively, by solid, dashed, and dotted curves. As shown in Fig. 5(f), the value of $E(\hat{x}_m,\hat{y}_m,\hat{z}_m)$ for the combination case of $(n_1,n_2,n_3,n_4,n_5,n_6) = (1,2,3,4,5,6)$ goes to zero monotonically.

To summarize, we have successfully obtained the stably converged solution $(\hat{x}_{100},\hat{y}_{100},\hat{z}_{100}) \simeq (\hat{x}*,\hat{y}*,\hat{z}*)$, at the 100th iteration stage by comparing all 720 NCGM convergence curves and choosing the minimum-error case for imperfect corner cubes with relatively large and small structural errors.

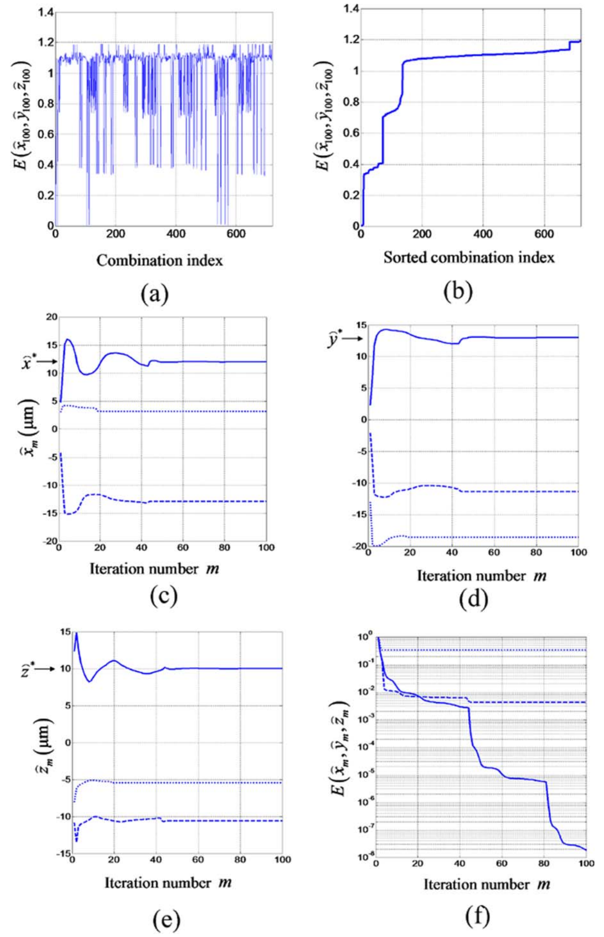

Fig. 4. (Color online) NCGM structure analysis result of an imperfect corner cube with $(\hat{x}*,\hat{y}*,\hat{z}*) = (12\,\mu\text{m},13\,\mu\text{m},10\,\mu\text{m})$: (a) plot of the error function values at the 100th iteration stage, $E(\hat{x}_{100},\hat{y}_{100},\hat{z}_{100})$, for the unsorted combination indices and (b) plot of the error function values for the sorted combination indices. Convergence curves for (c) $\hat{x}_m$, (d) $\hat{y}_m$, (e) $\hat{z}_m$, and (f) $E(\hat{x}_m,\hat{y}_m,\hat{z}_m)$ for the combination cases of $(n_1,n_2,n_3,n_4,n_5,n_6) = (1,2,3,4,5,6)$, $(n_1,n_2,n_3,n_4,n_5,n_6) = (5,4,6,2,1,3)$, and $(n_1,n_2,n_3,n_4,n_5,n_6) = (2,4,5,6,3,1)$ are indicated, respectively, by solid, dashed, and dotted curves.

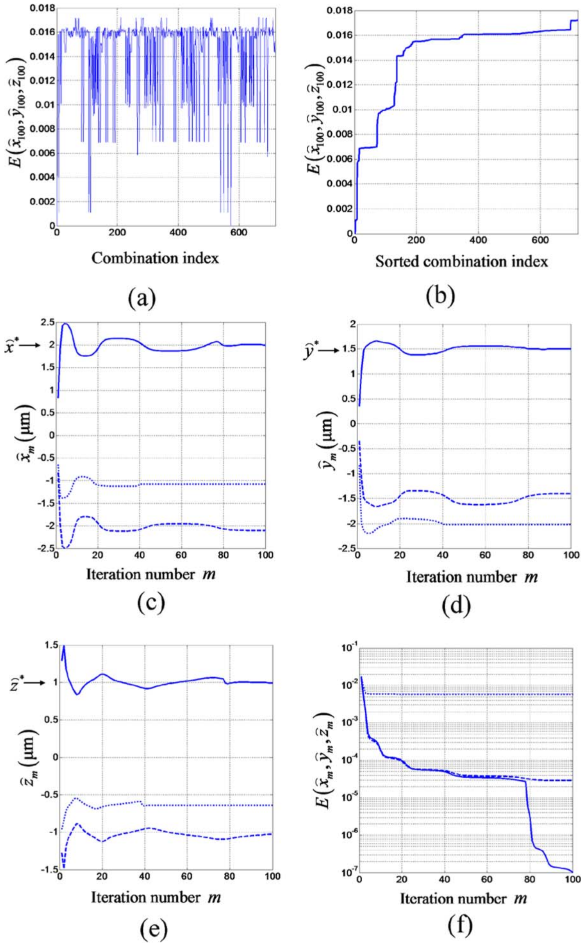

Fig. 5. (Color online) NCGM structure analysis result of an imperfect corner cube with $(\hat{x}*, \hat{y}*, \hat{z}*) = (2\,\mu\text{m}, 1.5\,\mu\text{m}, 1\,\mu\text{m})$: (a) plot of the error function values at the 100th iteration stage, $E(\hat{x}_{100}, \hat{y}_{100}, \hat{z}_{100})$ for the unsorted combination indices and (b) plot of the error function values for the sorted combination indices. Convergence curves for (c) $\hat{x}_m$, (d) $\hat{y}_m$, (e) $\hat{z}_m$, and (f) $E(\hat{x}_m, \hat{y}_m, \hat{z}_m)$ for the combination cases of $(n_1, n_2, n_3, n_4, n_5, n_6) = (1, 2, 3, 4, 5, 6)$, $(n_1, n_2, n_3, n_4, n_5, n_6) = (5, 4, 6, 2, 1, 3)$, and $(n_1, n_2, n_3, n_4, n_5, n_6) = (6, 4, 5, 2, 1, 3)$ are indicated, respectively, by solid, dashed, and dotted curves.

4. Conclusion

In conclusion, we have developed a geometrical optics structural analysis method for imperfect retroreflection corner cubes with the nonlinear conjugate gradient method (NCGM). The proposed method of analysis is a mathematical basis for the nondestructive optical inspection of imperfectly fabricated retroreflection corner cubes, since only the optically measurable six-beam reflection patterns are used in the analysis. The NCGM is implemented with the analytic expression of the gradient vector of the error function for analyzing the structural error of imperfect corner cube. Using the proposed method, we can simply and accurately evaluate the structural reliability of retroreflection corner cubes.

Appendix A: Structure of a Perfect Corner Cube

The perfect corner-cube structure is placed in the local coordinate system [23] shown in Fig. 6. In Fig. 6, the intercept points $(x_0, y_0, z_0)$are given by

$$(x_0, y_0, z_0) = \left(\sqrt{\frac{l_{12}^2 - l_{23}^2 + l_{13}^2}{2}}, \sqrt{\frac{l_{12}^2 + l_{23}^2 - l_{13}^2}{2}}, \times \sqrt{\frac{-l_{12}^2 + l_{23}^2 + l_{13}^2}{2}}\right), \tag{A1}$$

and the cross point of the incidence facet and its normal vector from the origin, (x_m, y_m, z_m), are given by

$$(x_m, y_m, z_m) = \frac{1}{(1/x_0)^2 + (1/y_0)^2 + (1/z_0)^2} \times (1/x_0, 1/y_0, 1/z_0). \tag{A2}$$

Then l_{14}, l_{24}, and l_{34} are given, respectively, by

$$l_{14} = \sqrt{(x_m - x_0)^2 + y_m^2 + z_m^2}, \tag{A3a}$$

$$l_{24} = \sqrt{(x_m^2 + (y_m - y_0)^2 + z_m^2}, \tag{A3b}$$

$$l_{34} = \sqrt{(x_m^2 + y_m^2 + (z_0 - z_m)^2}. \tag{A3c}$$

Then the coordinate $(\bar{x}_c, \bar{y}_c, -\bar{h})$ of the apex point of the perfect corner-cube structure is given by

$$\bar{x}_c = \frac{l_{12}^2 + l_{14}^2 - l_{24}^2}{2l_{12}}, \tag{A4a}$$

$$\bar{y}_c = \frac{\sqrt{(l_{12} + l_{24} + l_{14})(l_{12} - l_{24} + l_{14})(l_{12} + l_{24} - l_{14})(-l_{12} + l_{24} + l_{14})}}{2l_{12}}, \tag{A4b}$$

$$\bar{h}=\frac{1}{\sqrt{\left(\frac{1}{x_0}\right)^2+\left(\frac{1}{y_0}\right)^2+\left(\frac{1}{z_0}\right)^2}}$$
$$=\frac{1}{\sqrt{2}}\frac{\left(\sqrt{l_{12}^2-l_{23}^2+l_{13}^2}\sqrt{l_{12}^2+l_{23}^2-l_{13}^2}\sqrt{-l_{12}^2+l_{23}^2+l_{13}^2}\right)}{\sqrt{\left(\sqrt{l_{12}^2-l_{23}^2+l_{13}^2}\sqrt{l_{12}^2+l_{23}^2-l_{13}^2}\right)^2+\left(\sqrt{l_{12}^2+l_{23}^2-l_{13}^2}\sqrt{-l_{12}^2+l_{23}^2+l_{13}^2}\right)^2+\left(\sqrt{-l_{12}^2+l_{23}^2+l_{13}^2}\sqrt{l_{12}^2-l_{23}^2+l_{13}^2}\right)^2}}. \tag{A4c}$$

Appendix B: Derivation of the Reflection Transform Γ

The mirror reflection that occurs on a reflection surface of a corner cube is considered as a linear vector transform. As shown in Fig. 7, an incident ray with the direction vector of (k_x, k_y, k_z) is reflected by the plane described by $a_i x + b_i y + c_i z + d_i = 0$. The direction vector of the reflected ray is denoted by $(k_{r,x}, k_{r,y}, k_{r,z})$. The relationship between the incident wave and the reflection wave is given by

$$(k_{r,x}, k_{r,y}, k_{r,z}) = (k_x, k_y, k_z) - 2(a_i, b_i, c_i)\frac{(k_x, k_y, k_z)\cdot(a_i, b_i, c_i)}{(a_i^2+b_i^2+c_i^2)}. \tag{B1a}$$

Therefore, the canonical form of the normalized reflection transform is given by

$$\begin{pmatrix} k_{r,x} \\ k_{r,y} \\ k_{r,z} \end{pmatrix} = \frac{1}{a_i^2+b_i^2+c_i^2} \times \begin{pmatrix} -a_i^2+b_i^2+c_i^2 & -2a_ib_i & -2c_ia_i \\ -2a_ib_i & a_i^2-b_i^2+c_i^2 & -2b_ia \\ -2c_ia_i & -2b_ic_i & a_i^2+b_i^2+c_i^2 \end{pmatrix} \times \begin{pmatrix} k_x \\ k_y \\ k_z \end{pmatrix}. \tag{B1b}$$

Hence, $\mathbf{\Gamma}_1$, $\mathbf{\Gamma}_2$, and $\mathbf{\Gamma}_3$ are given by

$$\mathbf{\Gamma}_i = \begin{pmatrix} \frac{-a_i^2+b_i^2+c_i^2}{a_i^2+b_i^2+c_i^2} & \frac{-2a_ib_i}{a_i^2+b_i^2+c_i^2} & \frac{-2c_ia_i}{a_i^2+b_i^2+c_i^2} \\ \frac{-2a_ib_i}{a_i^2+b_i^2+c_i^2} & \frac{a_i^2-b_i^2+c_i^2}{a_i^2+b_i^2+c_i^2} & \frac{-2b_ic_i}{a_i^2+b_i^2+c_i^2} \\ \frac{-2c_ia_i}{a_i^2+b_i^2+c_i^2} & \frac{-2b_ic_i}{a_i^2+b_i^2+c_i^2} & \frac{a_i^2+b_i^2-c_i^2}{a_i^2+b_i^2+c_i^2} \end{pmatrix}, \quad \text{for } i = 1, 2, 3. \tag{B2}$$

Appendix C: Classification of Retroreflection by an Imperfect Corner Cube

Here, the classification of retroreflection by imperfect corner cube is elucidated with a mathematical analysis. Let the dihedral angles between T_1 and T_2, between T_2 and T_3, and between T_3 and T_1 be denoted θ_{12}, θ_{23}, and θ_{31}, respectively.

From Eqs. (2a)–(2c) and the definition of the inner product, we can obtain the following relationships:

$$\begin{aligned}&\sqrt{a_1^2+b_1^2+c_1^2}\sqrt{a_2^2+b_2^2+c_2^2}\cos\theta_{12}\\ &= (a_1, b_1, c_1)\cdot(a_2, b_2, c_2)\\ &= x_2(x_3-x_2)h^2 + x_2^2 y_3 y_c - x_2 y_3 x_c y_c - x_2(x_2-x_3)y_c^2,\end{aligned} \tag{C1a}$$

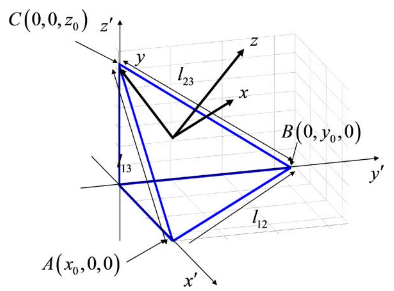

Fig. 6. (Color online) Schematics of a perfect corner cube in the local coordinate system (x', y', z').

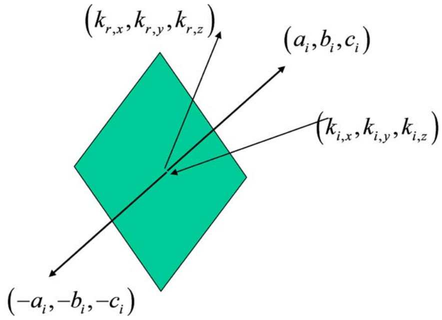

Fig. 7. (Color online) Reflection of a ray with incidence direction (k_x, k_y, k_z) by a plane $a_i x + b_i y + c_i z + d_i = 0$.

$$\begin{aligned}\sqrt{a_2^2+b_2^2+c_2^2}\sqrt{a_3^2+b_3^2+c_3^2}\cos\theta_{23} &= (a_2,b_2,c_2)\cdot(a_3,b_3,c_3)\\ &= [(-x_3+x_2)x_3-y_3^2]h^2\\ &\quad+[(x_2-x_3)x_3y_c^2-y_3^2x_c^2+(2x_3y_3-x_2y_3)x_cy_c\\ &\quad+x_cy_3^2x_c-x_2x_3y_3y_3],\end{aligned} \tag{C1b}$$

$$\begin{aligned}\sqrt{a_3^2+b_3^2+c_3^2}\sqrt{a_1^2+b_1^2+c_1^2}\cos\theta_{31} &= (a_3,b_3,c_3)\cdot(a_1,b_1,c_1)\\ &= -x_2x_3h^2-x_2x_3y_c^2+x_2y_3x_cy_c.\end{aligned} \tag{C1c}$$

We define the sets of the apex point $(x_c, y_c, -h)$ such that $\theta_{12} = 0$, $\theta_{23} = 0$, and $\theta_{31} = 0$, denoted Π_{12}, Π_{23}, and Π_{31}, respectively. With Eqs. (C1a)–(C1c), we obtain the mathematical expressions for Π_{12}, Π_{23}, and Π_{31}, respectively, as

$$\begin{aligned}\Pi_{12} &= \{(x_c,y_c,-h)|\cos\theta_{12}=0\}\\ &= \left\{(x_c,y_c,-h)|h^2=-y_c^2+\frac{x_2^2y_3y_c-x_2y_3x_cy_c}{x_2(x_2-x_3)}\right\},\end{aligned} \tag{C2a}$$

$$\begin{aligned}\Pi_{31} &= \{(x_c,y_c,-h)|\cos\theta_{31}=0\}\\ &= \left\{(x_c,y_c,-h)|h^2=-y_c^2+\frac{y_3}{x_3}x_cy_c\right\}.\end{aligned} \tag{C2c}$$

Based on the three sets defined above, we can classify the following eight possibilities: (i) $\cos\theta_{12} = 0$, $\cos\theta_{23} = 0$, and $\cos\theta_{31} = 0$; (ii) $\cos\theta_{12} \neq 0$, $\cos\theta_{23} = 0$, and $\cos\theta_{31} = 0$; (iii) $\cos\theta_{12} = 0$, $\cos\theta_{23} \neq 0$, and $\cos\theta_{31} = 0$; (iv) $\cos\theta_{12} = 0$, $\cos\theta_{23} = 0$, and $\cos\theta_{31} \neq 0$; (v) $\cos\theta_{12} = 0$, $\cos\theta_{23} \neq 0$, and $\cos\theta_{31} \neq 0$; (vi) $\cos\theta_{12} \neq 0$, $\cos\theta_{23} = 0$, and $\cos\theta_{31} \neq 0$; (vii) $\cos\theta_{12} \neq 0$, $\cos\theta_{23} \neq 0$, and $\cos\theta_{31} = 0$; and (viii) $\cos\theta_{12} \neq 0$, $\cos\theta_{23} \neq 0$, and $\cos\theta_{31} \neq 0$.

For case (i), $\cos\theta_{12} = 0$, $\cos\theta_{23} = 0$, and $\cos\theta_{31} = 0$, all six reflection transforms of Eqs. (7a)–(7f) become the same one, since $\mathbf{\Gamma}_1\mathbf{\Gamma}_2 = \mathbf{\Gamma}_2\mathbf{\Gamma}_1$, $\mathbf{\Gamma}_2\mathbf{\Gamma}_3 = \mathbf{\Gamma}_2\mathbf{\Gamma}_3$, and $\mathbf{\Gamma}_3\mathbf{\Gamma}_1 = \mathbf{\Gamma}_1\mathbf{\Gamma}_3$. The corner cube in this case is perfect, giving a perfect retroreflection, that is, the one-beam retroreflection.

For case (ii), $\cos\theta_{12} \neq 0$, $\cos\theta_{23} = 0$, and $\cos\theta_{31} = 0$, since $\mathbf{\Gamma}_2\mathbf{\Gamma}_3 = \mathbf{\Gamma}_3\mathbf{\Gamma}_2$ and $\mathbf{\Gamma}_3\mathbf{\Gamma}_1 = \mathbf{\Gamma}_1\mathbf{\Gamma}_3$, the six reflection transforms are divided into two groups, as $\mathbf{\Gamma}_1\mathbf{\Gamma}_2\mathbf{\Gamma}_3 = \mathbf{\Gamma}_1\mathbf{\Gamma}_3\mathbf{\Gamma}_2 = \mathbf{\Gamma}_3\mathbf{\Gamma}_1\mathbf{\Gamma}_2$ and $\mathbf{\Gamma}_2\mathbf{\Gamma}_1\mathbf{\Gamma}_3 = \mathbf{\Gamma}_2\mathbf{\Gamma}_3\mathbf{\Gamma}_1 = \mathbf{\Gamma}_3\mathbf{\Gamma}_2\mathbf{\Gamma}_1$. This means that the imperfect corner cube in this case produces a two-beam retroreflection. The set of the apex point in this case, $\Pi^{(2)}$, can be represented by $\Pi^{(2)} = \Pi_{12}^c \cap \Pi_{23} \cap \Pi_{31}$, where the superscript c of Π_{12}^c indicates the complementary set of Π_{12}. The trace of the apex point P_5 in $\Pi^{(2)}$ and the traces of two distinguished corresponding reflected rays on the hemispherical surface are shown in Figs. 8(a) and 8(b), respectively.

For case (iii), $\cos\theta_{12} = 0$, $\cos\theta_{23} \neq 0$, and $\cos\theta_{31} = 0$, since $\mathbf{\Gamma}_1\mathbf{\Gamma}_2 = \mathbf{\Gamma}_2\mathbf{\Gamma}_1$ and $\mathbf{\Gamma}_3\mathbf{\Gamma}_1 = \mathbf{\Gamma}_1\mathbf{\Gamma}_3$, the six reflection transforms are divided into two groups, as $\mathbf{\Gamma}_1\mathbf{\Gamma}_2\mathbf{\Gamma}_3 = \mathbf{\Gamma}_2\mathbf{\Gamma}_1\mathbf{\Gamma}_3 = \mathbf{\Gamma}_2\mathbf{\Gamma}_3\mathbf{\Gamma}_1$ and $\mathbf{\Gamma}_1\mathbf{\Gamma}_3\mathbf{\Gamma}_2 = \mathbf{\Gamma}_3\mathbf{\Gamma}_1\mathbf{\Gamma}_2 = \mathbf{\Gamma}_3\mathbf{\Gamma}_2\mathbf{\Gamma}_1$. And in case (iv), $\cos\theta_{12} = 0$, $\cos\theta_{23} = 0$, and $\cos\theta_{31} \neq 0$, since $\mathbf{\Gamma}_1\mathbf{\Gamma}_2 = \mathbf{\Gamma}_2\mathbf{\Gamma}_1$ and $\mathbf{\Gamma}_3\mathbf{\Gamma}_2 = \mathbf{\Gamma}_2\mathbf{\Gamma}_3$, the six reflection transforms are divided into two groups as $\mathbf{\Gamma}_1\mathbf{\Gamma}_2\mathbf{\Gamma}_3 = \mathbf{\Gamma}_2\mathbf{\Gamma}_1\mathbf{\Gamma}_3 = \mathbf{\Gamma}_1\mathbf{\Gamma}_3\mathbf{\Gamma}_2$ and $\mathbf{\Gamma}_3\mathbf{\Gamma}_2\mathbf{\Gamma}_1 = \mathbf{\Gamma}_2\mathbf{\Gamma}_3\mathbf{\Gamma}_1 = \mathbf{\Gamma}_3\mathbf{\Gamma}_1\mathbf{\Gamma}_2$.

By a manner similar to that in case (ii), we can see that two-beam retroreflection occurs in the imperfect corner cubes of cases (iii) and (iv). The sets of the apex points of (iii) and (iv), $\Pi^{(3)}$ and $\Pi^{(4)}$, are represented by $\Pi^{(3)} = \Pi_{12} \cap \Pi_{23}^c \cap \Pi_{31}$ and $\Pi^{(4)} = \Pi_{12} \cap \Pi_{23} \cap \Pi_{31}^c$, respectively. In Figs. 9(a) and 9(b), the trace of the apex point P_5 in $\Pi^{(3)}$ and the traces of two corresponding reflected rays on the hemi-

$$\begin{aligned}\Pi_{23} &= \{(x_c,y_c,-h)|\cos\theta_{23}=0\}\\ &= \left\{(x_c,y_c,-h)|h^2=\frac{[(x_2-x_3)x_3y_c^2-y_3^2x_c^2+(2x_3y_3-x_2y_3)x_cy_c+x_2y_3^2x_c-x_2x_3y_3y_c]}{[y_3^2-(-x_3+x_2)x_3]}\right\},\end{aligned} \tag{C2b}$$

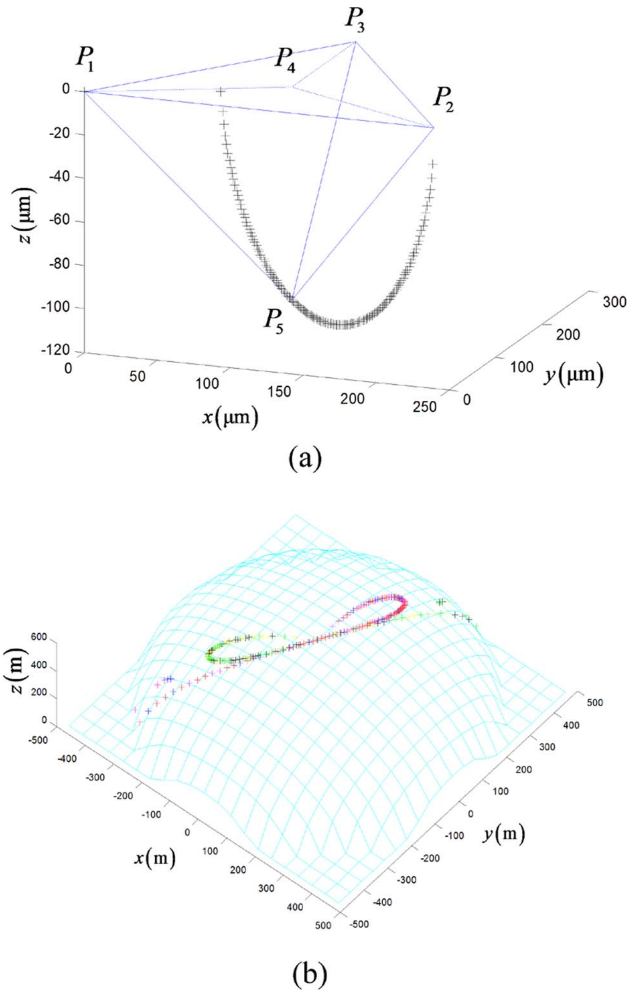

Fig. 8. (Color online) (a) Trace of the apex point P_5 in $\Pi^{(2)}$; (b) traces of two distinguished rays on the hemispherical surface for the case $\cos\theta_{12} \neq 0$, $\cos\theta_{23} = 0$, and $\cos\theta_{31} = 0$.

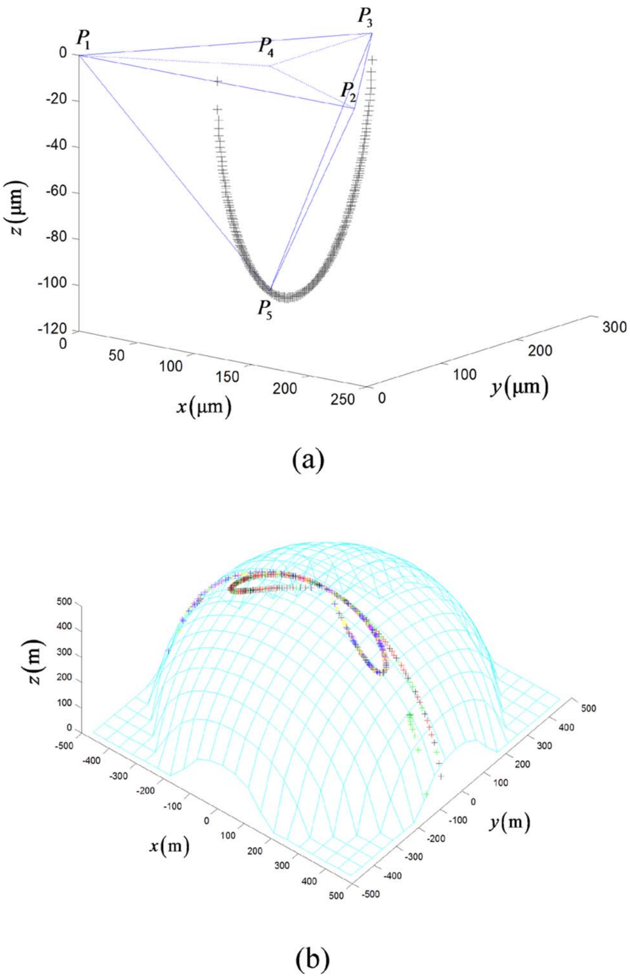

Fig. 9. (Color online) (a) Trace of the apex point P_5 in $\Pi^{(3)}$; (b) traces of two distinguished rays on the hemispherical surface for the case $\cos\theta_{12} = 0$, $\cos\theta_{23} \neq 0$, and $\cos\theta_{31} = 0$.

spherical surface are presented, respectively. In Figs. 10(a) and 10(b), the trace of the apex point P_5 in $\Pi^{(4)}$ and the traces of two distinguished reflected rays on the hemispherical surface are shown.

For case (v), $\cos\theta_{12} = 0$, $\cos\theta_{23} \neq 0$, and $\cos\theta_{31} \neq 0$, since $\mathbf{\Gamma}_1\mathbf{\Gamma}_2 = \mathbf{\Gamma}_2\mathbf{\Gamma}_1$, the six reflection transforms are divided into the four groups $\mathbf{\Gamma}_1\mathbf{\Gamma}_2\mathbf{\Gamma}_3 = \mathbf{\Gamma}_2\mathbf{\Gamma}_1\mathbf{\Gamma}_3$, $\mathbf{\Gamma}_3\mathbf{\Gamma}_2\mathbf{\Gamma}_1 = \mathbf{\Gamma}_3\mathbf{\Gamma}_1\mathbf{\Gamma}_2$, $\mathbf{\Gamma}_1\mathbf{\Gamma}_3\mathbf{\Gamma}_2$, and $\mathbf{\Gamma}_2\mathbf{\Gamma}_3\mathbf{\Gamma}_1$. Thus the imperfect corner cube in this case produces four-beam retroreflection. The set of the apex points for this case, $\Pi^{(5)}$, can be represented by $\Pi^{(5)} = \Pi_{12}\cap\Pi_{23}^c\cap\Pi_{31}^c$. In Figs. 11(a) and 11(b), the trace of the apex point P_5 in $\Pi^{(5)}$ and the traces of four distinguished reflected rays on the hemispherical surface are presented, respectively.

For case (vi), $\cos\theta_{12} \neq 0$, $\cos\theta_{23} = 0$, and $\cos\theta_{31} \neq 0$, since $\mathbf{\Gamma}_2\mathbf{\Gamma}_3 = \mathbf{\Gamma}_3\mathbf{\Gamma}_2$, the six reflection transforms are divided into four groups as $\mathbf{\Gamma}_1\mathbf{\Gamma}_2\mathbf{\Gamma}_3 = \mathbf{\Gamma}_1\mathbf{\Gamma}_3\mathbf{\Gamma}_2$, $\mathbf{\Gamma}_3\mathbf{\Gamma}_2\mathbf{\Gamma}_1 = \mathbf{\Gamma}_2\mathbf{\Gamma}_3\mathbf{\Gamma}_1$, $\mathbf{\Gamma}_2\mathbf{\Gamma}_1\mathbf{\Gamma}_3$, and $\mathbf{\Gamma}_3\mathbf{\Gamma}_1\mathbf{\Gamma}_2$. And for case (vii), $\cos\theta_{12} \neq 0$, $\cos\theta_{23} \neq 0$, and $\cos\theta_{31} = 0$, since $\mathbf{\Gamma}_2\mathbf{\Gamma}_3 = \mathbf{\Gamma}_3\mathbf{\Gamma}_2$, the six reflection transforms are divided into four groups as $\mathbf{\Gamma}_1\mathbf{\Gamma}_3\mathbf{\Gamma}_2 = \mathbf{\Gamma}_3\mathbf{\Gamma}_1\mathbf{\Gamma}_2$, $\mathbf{\Gamma}_2\mathbf{\Gamma}_3\mathbf{\Gamma}_1 = \mathbf{\Gamma}_2\mathbf{\Gamma}_1\mathbf{\Gamma}_3$, $\mathbf{\Gamma}_3\mathbf{\Gamma}_2\mathbf{\Gamma}_1$, and $\mathbf{\Gamma}_1\mathbf{\Gamma}_2\mathbf{\Gamma}_3$.

By in manner similar to that for case (v), we can see that four-beam retroreflection occurs in the imperfect corner cubes of cases (vi) and (vii). The sets of the apex points of (vi) and (vii), $\Pi^{(6)}$ and $\Pi^{(7)}$, are represented by $\Pi^{(6)} = \Pi_{23}^c\cap\Pi_{23}\cap\Pi_{31}^c$ and $\Pi^{(7)} = \Pi_{12}^c\cap\Pi_{23}^c\cap\Pi_{31}$, respectively. In Figs. 12(a) and 12(b), the trace of the apex point P_5 in $\Pi^{(6)}$ and the traces of four corresponding distinguished reflected rays on the hemispherical surface are shown, respectively. In Figs. 13(a) and 13(b), the trace of the apex point P_5 in $\Pi^{(7)}$ and the traces of four distinguished reflected rays on the hemispherical surface are presented, respectively.

Finally, for case (viii), $\cos\theta_{12} \neq 0$, $\cos\theta_{23} \neq 0$, and $\cos\theta_{31} \neq 0$, all six reflection transforms are different. Thus six-beam retroreflection occurs in the imperfect corner cubes of this case as presented in the main text (see Fig. 3).

Appendix D: Derivation of the Partial Derivatives, $\partial_{\hat{\mathbf{x}}(\hat{\mathbf{y}},\hat{\mathbf{z}})}\boldsymbol{\Gamma}_1$, $\partial_{\hat{\mathbf{x}}(\hat{\mathbf{y}},\hat{\mathbf{z}})}\boldsymbol{\Gamma}_2$, $\partial_{\hat{\mathbf{x}}(\hat{\mathbf{y}},\hat{\mathbf{z}})}\boldsymbol{\Gamma}_3$

The canonical form of the reflection transform takes the form

$$\mathbf{\Gamma} = \begin{pmatrix} \frac{-a^2+b^2+c^2}{a^2+b^2+c^2} & \frac{-2ab}{a^2+b^2+c^2} & \frac{-2ca}{a^2+b^2+c^2} \\ \frac{-2ab}{a^2+b^2+c^2} & \frac{a^2-b^2+c^2}{a^2+b^2+c^2} & \frac{-2bc}{a^2+b^2+c^2} \\ \frac{-2ca}{a^2+b^2+c^2} & \frac{-2bc}{a^2+b^2+c^2} & \frac{a^2+b^2-c^2}{a^2+b^2+c^2} \end{pmatrix}. \tag{D1}$$

The total derivative of $\mathbf{\Gamma}$ is given by

$$\Delta\mathbf{\Gamma} = \Delta \begin{pmatrix} \frac{-a^2+b^2+c^2}{a^2+b^2+c^2} & \frac{-2ab}{a^2+b^2+c^2} & \frac{-2ca}{a^2+b^2+c^2} \\ \frac{-2ab}{a^2+b^2+c^2} & \frac{a^2-b^2+c^2}{a^2+b^2+c^2} & \frac{-2bc}{a^2+b^2+c^2} \\ \frac{-2ca}{a^2+b^2+c^2} & \frac{-2bc}{a^2+b^2+c^2} & \frac{a^2+b^2-c^2}{a^2+b^2+c^2} \end{pmatrix}, \tag{D2a}$$

whose elements are given, respectively, by

$$\Delta\left(\frac{-a^2+b^2+c^2}{a^2+b^2+c^2}\right) = \frac{\Delta a(4a(b^2+c^2)) + \Delta b(-4ba^2) + \Delta c(-4ca^2)}{(a^2+b^2+c^2)^2}, \tag{D2b}$$

$$\Delta\left(\frac{a^2-b^2+c^2}{a^2+b^2+c^2}\right) = \frac{\Delta a(-4ab^2) + \Delta b(4b(c^2+a^2)) + \Delta c(-4cb^2)}{(a^2+b^2+c^2)^2}, \tag{D2c}$$

$$\Delta\left(\frac{a^2+b^2-c^2}{a^2+b^2+c^2}\right) = \frac{\Delta a(-4ac^2) + \Delta b(-4bc^2) + \Delta c(4c(a^2+b^2))}{(a^2+b^2+c^2)^2}, \tag{D2d}$$

$$\Delta\left(\frac{-2ab}{a^2+b^2+c^2}\right) = \frac{\Delta a(2b(-a^2+b^2+c^2)) + \Delta b(2a(a^2-b^2+c^2)) + \Delta c(-4abc)}{(a^2+b^2+c^2)^2}, \tag{D2e}$$

$$\Delta\left(\frac{-2ca}{a^2+b^2+c^2}\right) = \frac{\Delta a(2c(-a^2+b^2+c^2)) + \Delta b(-4abc) + \Delta c(2a(a^2+b^2-c^2))}{(a^2+b^2+c^2)^2}, \tag{D2f}$$

$$\Delta\left(\frac{-2bc}{a^2+b^2+c^2}\right) = \frac{\Delta a(-4abc) + \Delta b(2c(a^2-b^2+c^2)) + \Delta c(2b(a^2+b^2-c^2))}{(a^2+b^2+c^2)^2}. \tag{D2g}$$

Let us recall that $(x_c, y_c, -h) = (\bar{x}_c + \hat{x}, \bar{y}_c + \hat{y}, -(\bar{h} + \hat{z}))$; then, with respect to $\mathbf{\Gamma}_1$, since $(a_1, b_1, c_1) = (0, -x_2h, -x_2y_c)$, the partial derivatives $\partial_{\hat{x}}(a_1, b_1, c_1)$, $\partial_{\hat{y}}(a_1, b_1, c_1)$, and $\partial_{\hat{z}}(a_1, b_1, c_1)$ are given, respectively, by

$$\partial_{\hat{x}}(a_1, b_1, c_1) = \lim_{\Delta\hat{x}\to 0}(\Delta a_1/\Delta\hat{x}, \Delta b_1/\Delta\hat{x}, \Delta c_1/\Delta\hat{x}) = (0, 0, 0), \tag{D3a}$$

$$\partial_{\hat{y}}(a_1, b_1, c_1) = \lim_{\Delta\hat{y}\to 0}(\Delta a_1/\Delta\hat{y}, \Delta b_1/\Delta\hat{y}, \Delta c_1/\Delta\hat{y}) = (0, 0, -x_2), \tag{D3b}$$

$$\partial_{\hat{z}}(a_1, b_1, c_1) = \lim_{\Delta\hat{z}\to 0}(\Delta a_1/\Delta\hat{z}, \Delta b_1/\Delta\hat{z}, \Delta c_1/\Delta\hat{z}) = (0, -x_2, 0). \tag{D3c}$$

In the same way, for $(a_2, b_2, c_2) = (y_3h, (-x_3 + x_2)h, -x_2y_3 + y_3x_c + (x_2 - x_3)y_c)$, and $(a_3, b_3, c_3) = (-y_3h,$

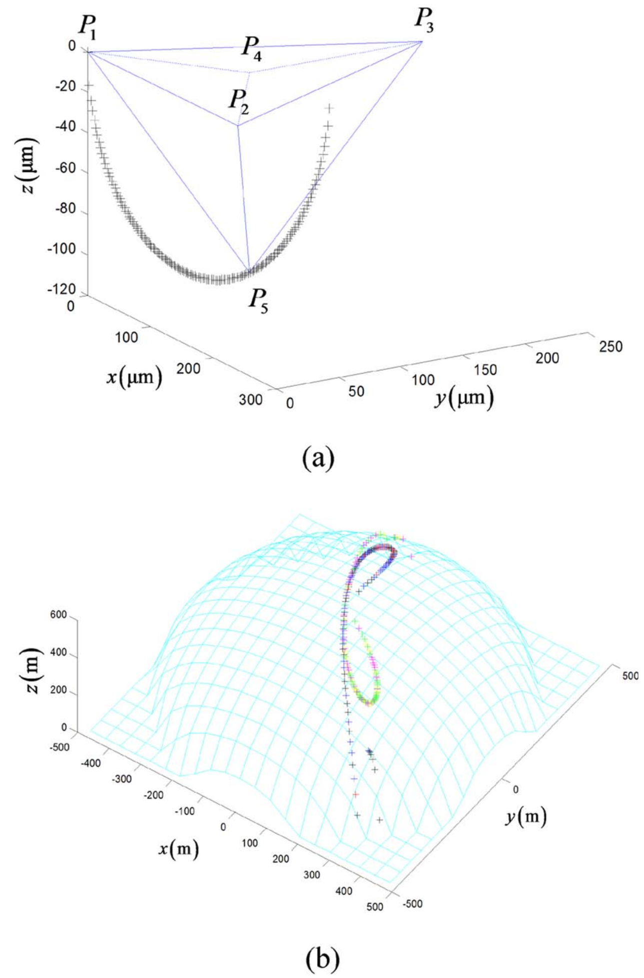

Fig. 10. (Color online) (a) Trace of the apex point P_5 in $\Pi^{(4)}$; (b) traces of two distinguished rays on the hemispherical surface for the case $\cos\theta_{12} = 0$, $\cos\theta_{23} = 0$, and $\cos\theta_{31} \neq 0$.

$x_3 h, y_c x_3 - y_3 x_c)$, the partial derivatives $\partial_{\hat{x}}(a_2, b_2, c_2)$, $\partial_{\hat{y}}(a_2, b_2, c_2)$, and $\partial_{\hat{z}}(a_2, b_2, c_2)$ are given, respectively, as

$$\partial_{\hat{x}}(a_2, b_2, c_2) = \lim_{\Delta\hat{x}\to 0}(\Delta a_2/\Delta\hat{x}, \Delta b_2/\Delta\hat{x}, \Delta c_2/\Delta\hat{x}) = (0, 0, y_3), \quad \text{(D4a)}$$

$$\partial_{\hat{y}}(a_2, b_2, c_2) = \lim_{\Delta\hat{y}\to 0}(\Delta a_2/\Delta\hat{y}, \Delta b_2/\Delta\hat{y}, \Delta c_2/\Delta\hat{y}) = (0, 0, x_2 - x_3), \quad \text{(D4b)}$$

$$\partial_{\hat{z}}(a_2, b_2, c_2) = \lim_{\Delta\hat{z}\to 0}(\Delta a_2/\Delta\hat{z}, \Delta b_2/\Delta\hat{z}, \Delta c_2/\Delta\hat{z}) = (y_3, -x_3 + x_2, 0). \quad \text{(D4c)}$$

And the partial derivatives, $\partial_{\hat{x}}(a_3, b_3, c_3)$, $\partial_{\hat{y}}(a_3, b_3, c_3)$, and $\partial_{\hat{z}}(a_3, b_3, c_3)$ are given, respectively, as

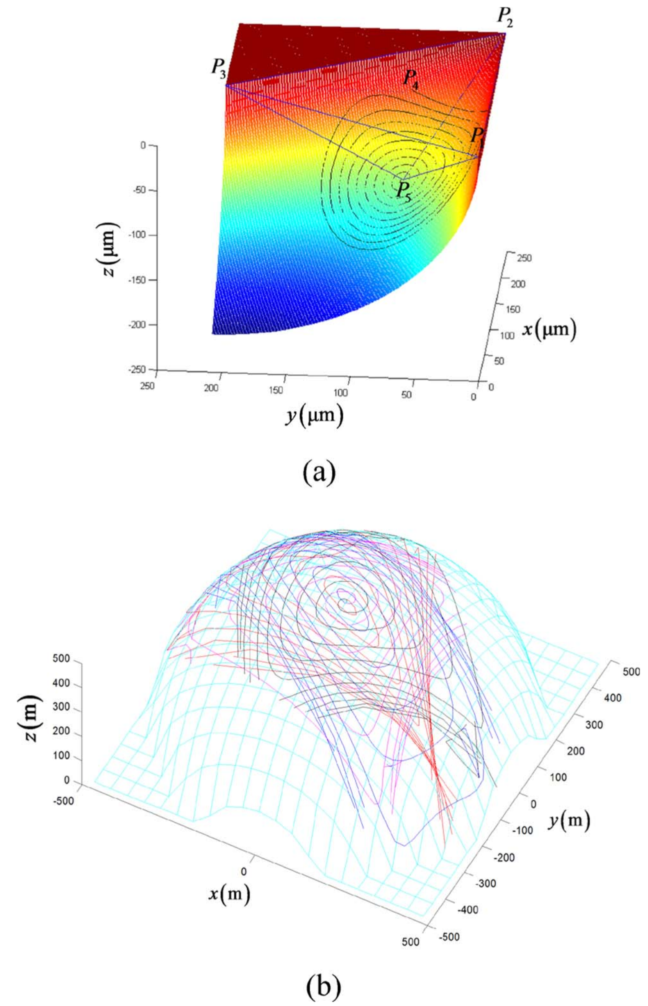

Fig. 11. (Color online) (a) Trace of the apex point P_5 in $\Pi^{(5)}$; (b) traces of four distinguished rays (blue, pink, red, and black) on the hemispherical surface for the case $\cos\theta_{12} = 0$, $\cos\theta_{23} \neq 0$, and $\cos\theta_{31} \neq 0$.

$$\partial_{\hat{x}}(a_3, b_3, c_3) = \lim_{\Delta\hat{x}\to 0}(\Delta a_3/\Delta\hat{x}, \Delta b_3/\Delta\hat{x}, \Delta c_3/\Delta\hat{x}) = (0, 0, -y_3), \quad \text{(D5a)}$$

$$\partial_{\hat{y}}(a_3, b_3, c_3) = \lim_{\Delta\hat{y}\to 0}(\Delta a_3/\Delta\hat{y}, \Delta b_3/\Delta\hat{y}, \Delta c_3/\Delta\hat{y}) = (0, 0, -x_3), \quad \text{(D5b)}$$

$$\partial_{\hat{z}}(a_3, b_3, c_3) = \lim_{\Delta\hat{z}\to 0}(\Delta a_3/\Delta\hat{z}, \Delta b_3/\Delta\hat{z}, \Delta c_3/\Delta\hat{z}) = (-y_3, x_3, 0). \quad \text{(D5c)}$$

By substituting Eqs. (D3a)–(D3c) into the canonical form of Eqs. (D2a)–(D2g), we obtain the partial derivatives $\partial_{\hat{x}}\mathbf{\Gamma}_1$, $\partial_{\hat{y}}\mathbf{\Gamma}_1$, and $\partial_{\hat{z}}\mathbf{\Gamma}_1$ as

$$\partial_{\hat{x}}\mathbf{\Gamma}_1 = \begin{pmatrix} 0 & 0 & 0 \\ 0 & 0 & 0 \\ 0 & 0 & 0 \end{pmatrix}, \tag{D6a}$$

$$\partial_{\hat{y}}\mathbf{\Gamma}_1 = \frac{1}{(a_1^2+b_1^2+c_1^2)^2}\begin{pmatrix} -x_2(-4c_1a_1^2) & -x_2(-4a_1b_1c_1) & -x_2(2a_1(a_1^2+b_1^2-c_1^2)) \\ -x_2(-4a_1b_1c_1) & -x_2(-4c_1b_1^2) & -x_2(2b_1(a_1^2+b_1^2-c_1^2)) \\ -x_2(2a_1(a_1^2+b_1^2-c_1^2)) & -x_2(2b_1(a_1^2+b_1^2-c_1^2)) & -x_2(4c_1(a_1^2+b_1^2)) \end{pmatrix}, \tag{D6b}$$

$$\partial_{\hat{z}}\mathbf{\Gamma}_1 = \frac{1}{(a_1^2+b_1^2+c_1^2)^2}\begin{pmatrix} -x_2(-4b_1a_1^2) & -x_2(2a_1(a_1^2-b_1^2+c_1^2)) & -x_2(-4a_1b_1c_1) \\ -x_2(2a_1(a_1^2-b_1^2+c_1^2)) & -x_2(4b_1(c_1^2+a_1^2)) & -x_2(2c_1(a_1^2-b_1^2+c_1^2)) \\ -x_2(-4a_1b_1c_1) & -x_2(2c_1(a_1^2-b_1^2+c_1^2)) & -x_2(-4b_1c_1^2) \end{pmatrix}. \tag{D6c}$$

By substituting Eqs. (D4a)–(D4c) into Eqs. (D2a)–(D2g), we obtain the partial derivatives $\partial_{\hat{x}}\mathbf{\Gamma}_2$, $\partial_{\hat{y}}\mathbf{\Gamma}_2$, and $\partial_{\hat{z}}\mathbf{\Gamma}_2$ as

$$\partial_{\hat{x}}\mathbf{\Gamma}_2 = \frac{1}{(a_2^2+b_2^2+c_2^2)^2}\begin{pmatrix} y_3(-4c_2a_2^2) & y_3(-4a_2b_2c_2) & y_3(2b_2(a_2^2+b_2^2-c_2^2)) \\ y_3(-4a_2b_2c_2) & y_3(-4c_2b_2^2) & y_3(2b_2(a_2^2+b_2^2-c_2^2)) \\ y_3(2a_2(a_2^2+b_2^2-c_2^2) & y_3(2b_2(a_2^2+b_2^2-c_2^2) & y_3(4c_2(a_2^2+b_2^2)) \end{pmatrix}, \tag{D7a}$$

$$\partial_{\hat{y}}\mathbf{\Gamma}_2 = \frac{1}{(a_2^2+b_2^2+c_2^2)^2}\begin{pmatrix} (x_2-x_3)(-4c_2a_2^2) & (x_2-x_3)(-4a_2b_2c_2) & (x_2-x_3)(2a_2(a_2^2+b_2^2-c_2^2)) \\ (x_2-x_3)(-4a_2b_2c_2) & (x_2-x_3)(-4c_2b_2^2) & (x_2-x_3)(2b_2(a_2^2+b_2^2-c_2^2)) \\ (x_2-x_3)(2a_2(a_2^2+b_2^2-c_2^2)) & (x_2-x_3)(2b_2(a_2^2+b_2^2-c_2^2) & (x_2-x_3)(4c_2(a_2^2+b_2^2)) \end{pmatrix}, \tag{D7b}$$

$$\partial_{\hat{z}}\mathbf{\Gamma}_2 = \frac{1}{(a_2^2+b_2^2+c_2^2)^2} \times \begin{pmatrix} y_3(4a_2(b_2^2+c_2^2)) + (-x_3+x_2)(-4b_2a_2^2) & y_3(2b_2(-a_2^2+b_2^2+c_2^2)) + (-x_3+x_2)(2a_2(a_2^2-b_2^2+c_2^2)) & y_3(2c_2(-a_2^2+b_2^2+c_2^2)) + (-x_3+x_2)(-4a_2b_2c_2) \\ y_3(2b_2(-a_2^2+b_2^2+c_2^2)) + (-x_3+x_2)(2a_2(a_2^2-b_2^2+c_2^2)) & y_3(-4a_2b_2^2) + (-x_3+x_2)(4b_2(c_2^2+a_2^2)) & y_3(-4a_2b_2c_2) + (-x_3+x_2)(2c_2(a_2^2-b_2^2+c_2^2)) \\ y_3(2c_2(-a_2^2+b_2^2+c_2^2)) + (-x_3+x_2)(-4a_2b_2c_2) & y_3(-4a_2b_2c_2) + (-x_3+x_2)(2c_2(a_2^2-b_2^2+c_2^2)) & y_3(-4a_2c_2^2) + (-x_3+x_2)(-4b_2c_2^2) \end{pmatrix}. \tag{D7c}$$

By substituting Eqs. (D5a)–(D5c) into Eqs. (D2a)–(D2g), we obtain the partial derivatives $\partial_{\hat{x}}\mathbf{\Gamma}_3$, $\partial_{\hat{y}}\mathbf{\Gamma}_3$, and $\partial_{\hat{z}}\mathbf{\Gamma}_3$ as

$$\partial_{\hat{x}}\mathbf{\Gamma}_3 = \frac{1}{(a_3^2+b_3^2+c_3^2)^2}\begin{pmatrix} -y_3(-4c_3a_3^2) & -y_3(-4a_3b_3c_3) & -y_3(2a_3(a_3^2+b_3^2-c_3^2)) \\ -y_3(-4a_3b_3c_3) & -y_3(-4c_3b_3^2) & -y_3(2b_3(a_3^2+b_3^2-c_3^2)) \\ -y_3(2a_3(a_3^2+b_3^2-c_3^2) & -y_3(2b_3(a_3^2+b_3^2-c_3^2) & -y_3(4c_3(a_3^2+b_3^2)) \end{pmatrix}, \tag{D8a}$$

$$\partial_{\hat{y}}\mathbf{\Gamma}_3 = \frac{1}{(a_3^2+b_3^2+c_3^2)^2}\begin{pmatrix} x_3(-4c_3a_3^2) & x_3(-4a_3b_3c_3) & x_3(2a_3(a_3^2+b_3^2-c_3^2)) \\ x_3(-4a_3b_3c_3) & x_3(-4c_3b_3^2) & x_3(2b_3(a_3^2+b_3^2-c_3^2)) \\ x_3(2a_3(a_3^2+b_3^2-c_3^2)) & x_3(2b_3(a_3^2+b_3^2-c_3^2)) & x_3(4c_3(a_3^2+b_3^2)) \end{pmatrix}, \tag{D8b}$$

$$\partial_{\hat{z}}\mathbf{\Gamma}_3 = \frac{1}{(a_3^2+b_3^2+c_3^2)^2} \times \begin{pmatrix} -y_3(4a_3(b_3^2+c_3^2))+x_3(-4b_3a_3^2) & -y_3(2b_3(-a_3^2+b_3^2+c_3^2))+x_3(2a_3(a_3^2-b_3^2+c_3^2)) & -y_3(2c_3(-a_3^2+b_3^2+c_3^2))+x_3(-4a_3b_3c_3) \\ -y_3(2b_3(-a_3^2+b_3^2+c_3^2))+x_3(2a_3(a_3^2-b_3^2+c_3^2)) & -y_3(-4a_3b_3^2)+x_3(4b_3(c_3^2+a_3^2)) & -y_3(-4a_3b_3c_3)+x_3(2c_3(a_3^2-b_3^2+c_3^2)) \\ -y_3(2c_3(-a_3^2+b_3^2+c_3^2))+x_3(-4a_3b_3c_3) & -y_3(-4a_3b_3c_3)+x_3(2c_3(a_3^2-b_3^2+c_3^2)) & -y_3(-4a_3c_3^2)+x_3(-4b_3c_3^2) \end{pmatrix}. \tag{D8c}$$

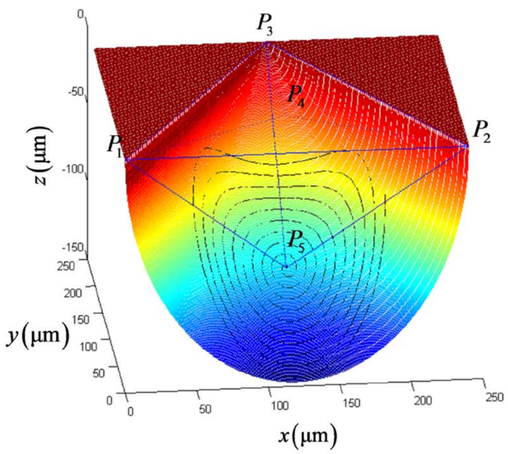

(a)

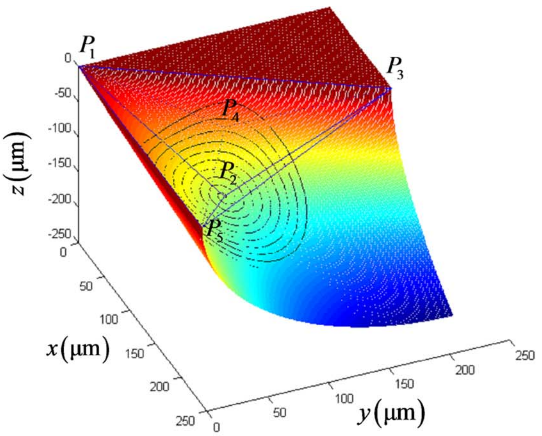

(a)

Fig. 13. (Color online) (a) Trace of the apex point P_5 in $\Pi^{(7)}$; (b) traces of four distinguished rays (blue, pink, red, and black) on the hemispherical surface for the case $\cos\theta_{12} \neq 0$, $\cos\theta_{23} \neq 0$, and $\cos\theta_{31} = 0$.

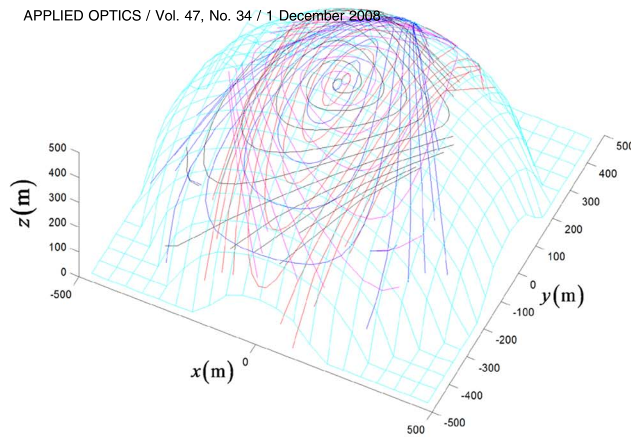

(b)

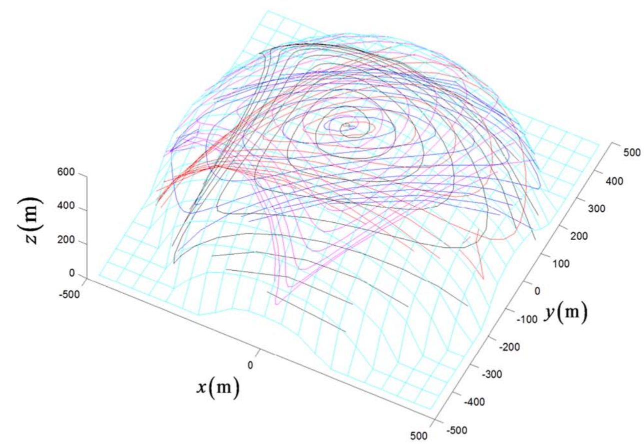

(b)

Fig. 12. (Color online) (a) Trace of the apex point P_5 in $\Pi^{(6)}$; (b) traces of four distinguished rays (blue, pink, red, and black) on the hemispherical surface for the case $\cos\theta_{12} \neq 0$, $\cos\theta_{23} = 0$, and $\cos\theta_{31} \neq 0$.

This work was supported by the Brain Korea 21 Program (Information Technology, Seoul National University).

References

1. *Retroreflection: Definition and Measurement*, Publ. CIE 54.202001 (Commission International de L'Eclairage, (2001).
2. R. B. Nilsen and X. J. Lu, "Retroreflection technology," Proc. SPIE **5616**, 47–60 (2004).
3. D. C. O'Brien, G. E. Faulkner, and D. J. Edwards, "Optical properties of a retroreflecting sheet," Appl. Opt. **38**, 4137–4144 (1999).
4. G. H. Seward and P. S. Cort, "Measurement and characterization of angular reflectance for cube-corners and microspheres," Opt. Eng. **38**, 164–169 (1999).
5. S. E. Segre and V. Zanza, "Mueller calculus polarization change in the cube-corner retroreflector," J. Opt. Soc. Am. A **20**, 1804–1811 (2003).
6. W. H. Venable and N. L. Johnson, "Unified coordinate system for retroreflectance measurements," Appl. Opt. **19**, 1236–1241 (1980).
7. A. Lundvall and F. Nikolajeff, "High performing micromachined retroreflector," Opt. Express **11**, 2459–2473 (2003).
8. K. Hyyppa, "Signal response of a laser beam scanner," Opt. Eng. **33**, 2770–2776 (1994).
9. O. Nakamara, M. Goto, K. Toyoda, N. Takai, T. Kurosawa, and T. Nakamata, "A laser tracking robot-performance calibration system using ball-seated bearing mechanisms and a spherically shaped cat's eye retro-reflector," Rev. Sci. Instrum. **65**, 1006–1011 (1994).
10. B. E. Hines, "Optical truss and retroreflector modeling for picometer laser metrology," Proc. SPIE **1947**, 198–208 (1993).
11. R. A. Chipman, J. Shamir, H. J. Caulfield, and Q. Zhou, "Wavefront correcting properties of corner-cube arrays," Appl. Opt. **27**, 3203–3209 (1996).
12. K. S. J. Pister, D. S. Gunawan, and L. Lin, "Micromachined corner cube reflectors as a communication link," Sens. Actuators A **47**, 580–583 (1995).
13. *Standard Specification for Retroreflective Sheeting for Traffic Control*, Publ. ASTM D 4956-0 (ASTM International, 2001).
14. *Product Catalog for Traffic Control Materials* (3M Traffic Control Materials Division, 2003), http://www.3M.com/tcm.
15. T. L. Hoopman, "Cube-corner retroreflective articles having wide angularity in multiple viewing planes," U.S. Patent 4,588,258 (13 May1986).
16. R. Fisher, "Head-mounted projection display system featuring beam splitter and method of making same," U.S. Patent 5,572,229 (5 November 1996).
17. H. Hua, A. Girardot, C. Gao, and J. P. Rolland "Engineering of head-mounted projective displays," Appl. Opt. **39**, 3814–3824 (2000).
18. J. Fergason. "Optical system for head mounted display using retro-reflector and method of displaying an image," U.S. Patent 5,621,572 (15 April 1997).
19. R. Kijima and T. Ojika, "Transition between virtual environment and workstation environment with projective head-mounted display," in *IEEE 1997 Virtual Reality Annual International Symposium* (IEEE, 1997), pp. 130–137.
20. M. Inami, N. Kawakami, D. Sekiguchi, Y. Yanagida, T. Maeda, and S. Tachi, "Visuo-haptic display using head-mounted projector," in *IEEE 2000 Virtual Reality Annual International Symposium* (IEEE, 2000), pp. 233–240.
21. H. Hua, C. Gao, F. Biocca, and J. P. Rolland, "An ultra-light and compact design and implementation of head-mounted projective displays," in *IEEE 2000 Virtual Reality Annual International Symposium* (IEEE, 2001), 175–182.
22. H. Hua, L. Brown, and C. Gao, "SCAPE: supporting stereoscopic collaboration in augmented and projective environments," IEEE Comput. Graphics Appl. **24**, 66–75 (2004).
23. H. Kim and B. Lee, "Optimal design of retroreflection cornercube sheets by geometric optics analysis," Opt. Eng. **45**, 094002 (2007).
24. C. T. Kelly, *Iterative Methods for Optimization, Frontiers in Applied Mathematics* (Society for Industrial and Applied Mathematics, 1999).
25. W. H. Press, B. P. Flannery, S. A. Teukolsky, and W. T. Vetterling, *Numerical Recipes in C: The Art of Scientific Computing* (Cambridge U. Press, 1992).